4. Results and Discussions

4.1 Material Composition

Table 4 and Table 5 present the elemental analysis of the starting material. Table 6 shows the mineralogical results. The results were obtained by XRF for elemental composition and XRD for mineralogical analysis.

Table 4: Composition of ilmenite raw material (major elements)

Component	SiO_2	TiO_2	Al_2O_3	Fe_2O_3	MnO	MgO	CaO	Na_2O
Concentration	0.48%	47.3%	0.51%	51.6%	0.97%	0.70%	0.07%	0.42%
Component	K_2O	P_2O_5	Cr_2O_3	NiO	V_2O_5	ZrO_2	**LOI**	**Total**
Concentration	0.02%	0.01%	0.17%	0.03%	0.51%	0.38%	-2.90	100

The elemental analysis indicated titanium and iron as the main constituents. This ore contains chromium, phosphorus and vanadium, which are impurities harmful to the quality. Niobium must be reduced as well during processing. The level of alkaline earth elements, namely magnesium and calcium, is found to be above the recommended level (Aminesh *et al.*, 2005; Habashi, 1997; Hollitt *et al.*, 2002; Lahiri *et al.*, 2006; Nielsen and Chang, 1996).

According to results from Table 1 and Table 2, the ore can be considered sulfate grade ilmenite. It is not suitable for chlorination due its low TiO_2 content (Murphy and Frick, 2006).

Table 5: Composition of ilmenite raw material (minor elements)

Element	**As**	**Cu**	**Ga**	**Mo**	**Nb**	**Ni**	**Pb**	**Rb**
Conc., ppm	3	21	5	4	466	58	96	8
Element	**Sr**	**Th**	**U**	**W***	**Y**	**Zn**	**Zr**	**Cl***
Conc., ppm	2	87	15	149	90	286	3086	8
Element	**Co**	**Cr**	**F***	**S***	**Sc**	**V**		
Conc., ppm	190	1629	100	543	48	572		

* = Semi-quantitative analysis; Conc.= concentration; ppm = parts per million

Mineralogical analysis showed that the ilmenite sample has zircon and ferrous oxide (Fe_2O_3) as the main impurities. Traces of anatase and rutile are also present in the sample (Table 6).

Table 6: Phase composition of the ilmenite raw material

Phase	$FeTiO_3$	Fe_2O_3	$ZrSiO_4$	TiO_2 (rutile)	TiO_2 (anatase)
Observation	Major	Minor	Minor	Trace	Sub-trace

4.2 Thermogravimetric Analysis

The reaction of sodium hydroxide with ilmenite was followed by TGA/DTA thermal analysis. Figure 9 shows a TG/DTG curve recorded at a rate of 10 ^{o}C/min of sample prepared by mixing two moles of sodium hydroxide with one mole of ilmenite.

The TG curve (Figure 9) shows an intense mass loss beginning just above 350 °C and ending at 525 °C. The observed mass loss is 6.53%, which is approximately 84% of the total expected if mass loss was due to dehydration of NaOH alone. In reality the mass gain due to oxidation must also be accounted for. The alkali fusion reaction of ilmenite is characterised by the evolution of water according to the following reaction (1):

$$4FeTiO_3 + 12NaOH + O_2 \rightarrow 4NaFeO_2 + 4Na_2TiO_3 + 6H_2O \quad (1)$$

On the DTG curve a maximum is observed at 490 °C for ilmenite reactant ($FeTiO_3$ in Figure 9). For ilmenite ore this value is shifted to 530 °C (ore in Figure 9). The DTG curve was constructed by differentiating the TG signal and plotting the obtained DTG results against temperature.

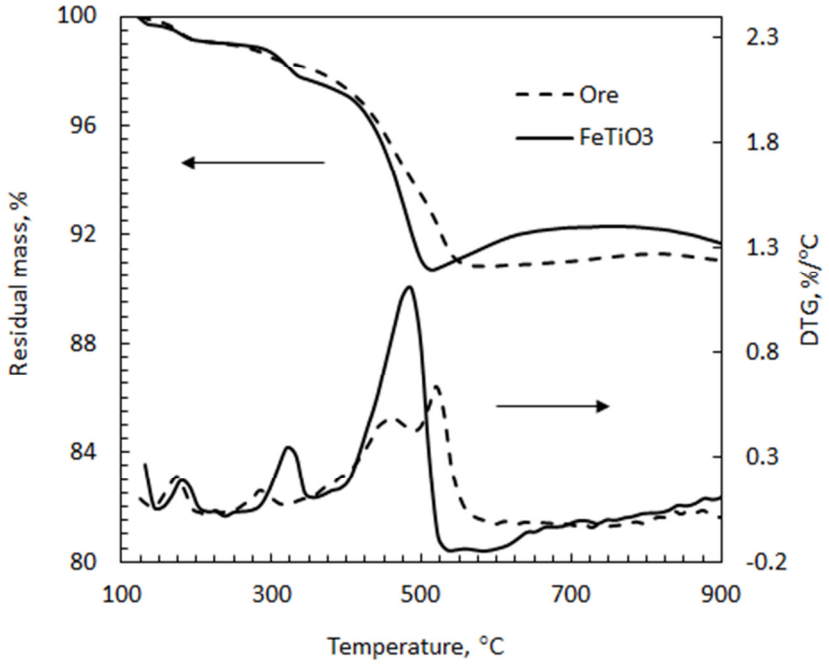

Figure 9:TG curves of the reaction of ilmenite ore and $FeTiO_3$ reactant (analytical grade) with two moles of NaOH (10 °C/min in oxygen)

With the ilmenite ore sample (Figure 9) the mass loss begins at comparatively lower temperatures, just above 200 to 560 °C. The stretching of the region corresponds to an overlapping of moisture release with water liberation from the reaction. The DTG curve shows a complex mechanism. This is an indication of two consecutive reactions with a large difference in the activation energy or in the frequency factor occurring (Wilburn, 2000). Two consecutive peaks, at 470 and 530 °C, are obtained. In this situation it is meaningless to determine the

activation energy values and the frequency factor, according to Wilburn (2000). Pure ilmenite (see Figure 9) shows a single peak in the DTG curve under similar conditions, at approximately 490 °C. This indicates that ilmenite itself reacts with NaOH in one single-step reaction with T_{max} ≈ 490 °C. This makes it possible to study the roasting reaction kinetically. The second reaction is believed to be that of other phases present as impurities in the ilmenite (see Table 4 and Table 5). The supplementary DTG peaks observed in the ilmenite ore curve were further investigated by heating mixtures of ilmenite ore and NaOH (2:1, NaOH:ilmenite mole ratio) and subjecting the product to XRD analysis for phases identification. Results are presented in Figure 10.

4.3 Fusion Results

4.3.1 Fusions at lower temperatures and extended periods

Experiments were performed at 250 and 500 °C. The identified phases in alkali fusion decomposed ilmenite (AFDI) in the XRD patterns are presented in Table 7.

Table 7: Identified phases in XRD patterns (Appendix A2–A6) of AFDI obtained after fusing for 336 h

Mol ratio (NaOH:$FeTiO_3$)	Temperature (°C)	Phases		
		$FeTiO_3$	Na_2TiO_3	Fe_2O_3
1:1	250	Major	-	-
2:1	250	Major	-	Minor
4:1	250	Major	-	-
6:1[8]	250	Major	-	-
4:1	500	Major	Major	Major[9]

In all samples sodium carbonate (Na_2CO_3) was present as the major phase. Sodium carbonate is a result of CO_2 absorption, by sodium hydroxide, from the atmosphere. Sodium silicate

[8] Amorphous
[9] As sodium iron silicon oxide, $Na_{0.925}(Fe_{0.925}Si_{0.075})O_2$

(Na_2SiO_3) and sodium iron silicate ($Na_{0,925}Fe_{0.925}Si_{0.075}O_2$) were observed at 500 °C, using four moles of sodium hydroxide per mole of ilmenite for 336 h.

The thermogravimetric results indicated that the reaction of ilmenite initiates just above 250 °C. The fusion experiments conducted at this temperature, using four different mole ratios (1:1, 2:1, 4:1 and 6:1, NaOH: $FeTiO_3$) for 336 h, did not produce noticeable changes (Appendix A2–A6, Table 1). At 500 °C, using four moles of NaOH, $FeTiO_3$ was still the dominant phase after 336 h of fusion. Na_2TiO_3 was the other major phase. $Na_{0.925}(Fe_{0.925}Si_{0.075})O_2$ was present as the concomitant iron phase (major). Silicon is incorporated, in a collateral reaction, in Fe^{3+} and Na^+ sites in $NaFeO_2$. The observed products are consistent with the following reaction (2):

$$4FeTiO_3 + 6Na_2O + O_2 \rightarrow 4Na_2TiO_3 + 4NaFeO_2 \quad (2)$$

4.3.2 Effect of fusion temperature

The effect of temperature was investigated using a 2:1 ($NaOH:FeTiO_3$) mole ratio. The temperature was varied from 300 to 950 °C, with a 50 °C gradient. The use of a 2:1 ($NaOH:FeTiO_3$) mole ratio is regarded as conducive to the formation of ternary phases and is economical in terms of NaOH consumption per mole of $FeTiO_3$. According to our results, Figure 10, no changes were observed at 300 °C. Ilmenite disappears from the products spectra only above 800 °C. Binary phases dominate below 600 °C, while ternary phases are observed above 650 °C. Figure 10 was plotted using the weight percent phase obtained as described in section 3.1.1. In order to minimize the number of phases presented in the graphic, for clarity, all the sodium titanate phases ($NaTiO_2$, $Na_8Ti_5O_{14}$ and Na_2TiO_3) were grouped as Na_2TiO_3. Sodium iron phases ($NaFeO_2.2H_2O$, $Fe_6(OH)_{12}CO_3.2H_2O$, and $NaFeO_2$) were grouped as $NaFeO_2$.

It is worth noting that the formation of ternary phases led to less NaOH being recovered. Figure 10 presents the identified phases in the XRD patterns (see Appendix A8–A19 and Table A 1). According to our results, no changes were observed at 300 °C. Ilmenite disappears from the products spectra only above 800 °C. Binary phases dominate below 600 °C, while ternary phases are observed above 650 °C.

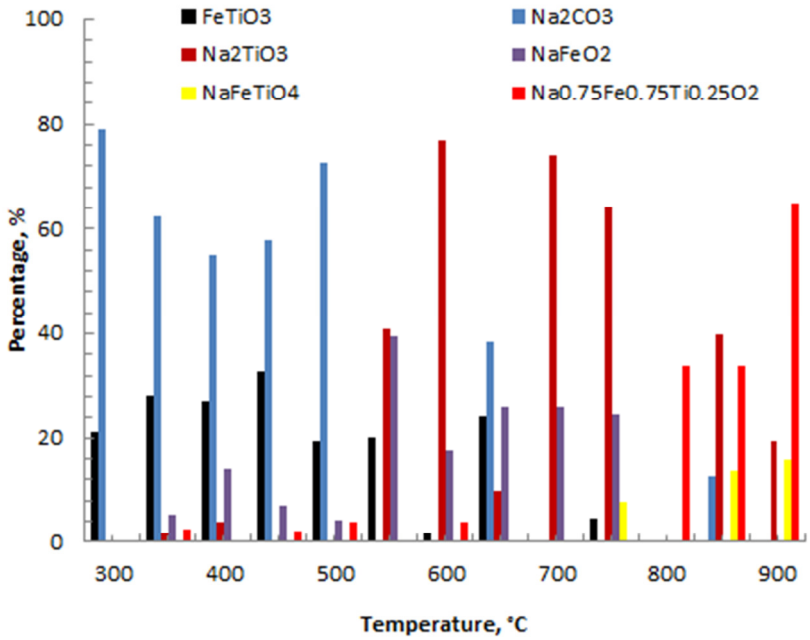

Figure 10: Effect of fusion temperature on the product spectra of the ilmenite alkali fusion reaction. Samples prepared with two mole NaOH per mole of ilmenite.

Five titanium-bearing phases were identified, namely $NaFeTiO_4$, $Na_8Ti_5O_{14}$, Na_2TiO_3, $Na_2Fe_2Ti_3O_{10}$ and $Na_{0.75}Fe_{0.75}Ti_{0.25}O_2$. No changes were detected at 300 °C. $Na_2Fe_2Ti_3O_{10}$ was observed only at 800 °C (Figure 11). Phases such as $Na_xFe_xTi_{2-x}O_4$, $Na_xFe_xTi_{8-x}O_{16}$, $Na_2Fe_2Ti_7O_{18}$, $NaFeTi_5O_{12}$, $Na_{2+x}Fe_xTi_{4-x}O_9$ and Na_4FeTiO_5 referred to in the literature were not observed in ourproducts (Bayer and Hoffman, 1965; Foley and Mackinnon, 1970; Li *et al.*, 1971; Reid and Sienko, 1967).

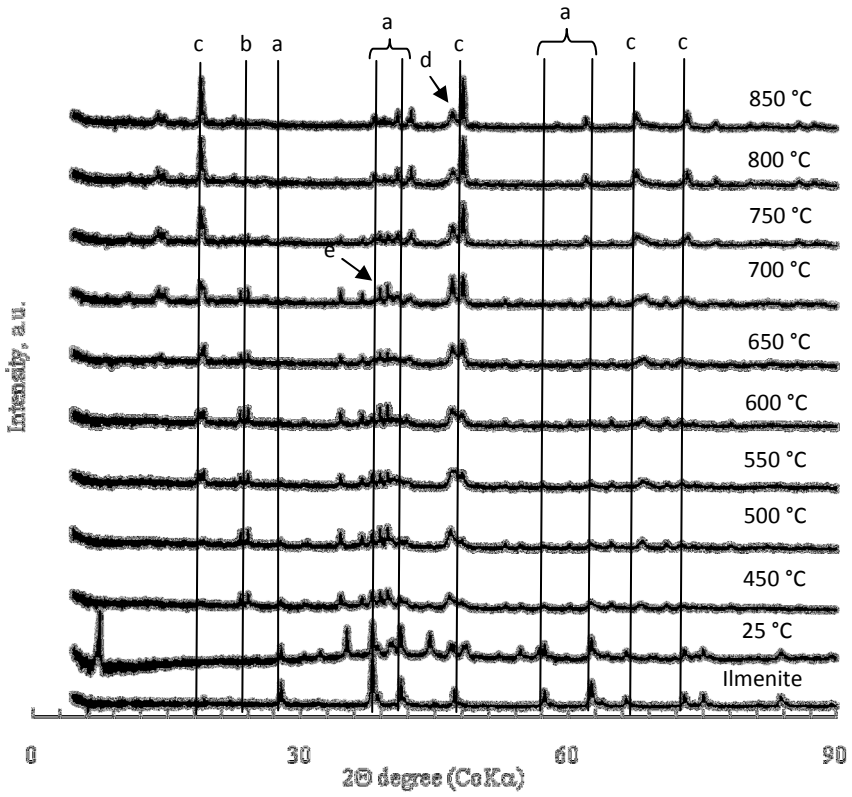

a = $FeTiO_4$; b = $NaFeO_2$; c = $Na_{0.75}Fe_{0.75}Ti_{0.25}O_2$; d = Na_2TiO_3; e = $NaFeTiO_4$

Figure 11: XRD difractograms of alkali fusion decomposed ilmenite. Samples of ilmenite:NaOH (2:1 mole ratio) were fused for 1 h at the indicated temperatures

Three temperature regions can be delimited in the reaction, according to the phases formed. From 350 to 550 °C, ilmenite is dominant, with $Na_{0.75}Fe_{0.75}Ti_{0.25}O_2$ as a minor phase. It is worth noting that Na_2CO_3 is also present as a major phase, indicating that the reaction was not completed under the conditions used. In two samples (at 350 and 400 °C) $NaTiO_2$ was detected. Its presence must be related to the non-availability of oxygen as oxidant, prompting to reduction of Ti^{4+} ions. $NaTiO_2$ is formed at the expense of Na_2TiO_3. Although single titanates, especially Na_2TiO_3, were not detected, the presence of $Na_{0.75}Fe_{0.75}Ti_{0.25}O_2$ and $NaFeO_2$ entails the formation of single titanates to accommodate the excess titanium. The Fe:Ti proportion in this phase is 3:1. The remaining Ti has to be accommodated in single titanates, mainly Na_2TiO_3. This is also supported by the findings of Foley and MacKinnon (1970). According to these

authors, when the Fe:Ti ratio is greater than 1:1 in the Na-Fe-Ti oxides, the surplus titania is accommodated as single titanates, mainly Na_2TiO_3. The presence of $NaFeO_2$ in the products is regarded as a collateral reaction of the Fe_2O_3 present in the sample as an impurity (see Table 6). The reaction (3) below the figure explains the observed transformations.

$$12FeTiO_3 + 14Na_2O + 3\ O_2 \rightarrow 16Na_{0.75}Fe_{0.75}Ti_{0.25}O_2 + 8Na_2TiO_3 \quad (3)$$

From 600 up to 800 °C a considerable proportion of $FeTiO_3$ was consumed. $Na_2Fe_2Ti_3O_{10}$, $NaFeTiO_4$, $Na_8Ti_5O_{14}$, Na_2TiO_3 and $Na_{0.75}Fe_{0.75}Ti_{0.25}O_2$ were detected in the products. $Na_8Ti_5O_{14}$, Na_2TiO_3 and $Na_{0.75}Fe_{0.75}Ti_{0.25}O_2$ were identified in the whole range of temperatures, while $NaFeTiO_4$ was identified at 750 and 800 °C. $Na_8Ti_5O_{14}$ tends to decrease with temperature, while Na_2TiO_3 and $Na_{0.75}Fe_{0.75}Ti_{0.25}O_2$ showed the opposite trend. This is in agreement with the findings of previous authors. $Na_8Ti_5O_{14}$ is involved in the Na_2TiO_3 formation reaction (Batygin, 1967; Belyaev *et al.*, 1970; Belyaev, 1976). The surplus iron was accommodated in $NaFeO_2$.

$NaFeO_2$ is present as a major phase in all samples. From these the following reaction was written (4):

$$16FeTiO_3 + 18Na_2O + 4O_2 \rightarrow 16Na_{0.75}Fe_{0.75}Ti_{0.25}O_2 + 2Na_2TiO_3 + 2Na_8Ti_5O_{14} + 4NaFeO_2 \quad (4)$$

From 850 to 950 °C ilmenite was completely consumed after the reaction time used. $NaFeTiO_4$, Na_2TiO_3 and $Na_{0.75}Fe_{0.75}Ti_{0.25}O_2$ are the only phases observed. $NaFeO_2$ is only observed at 850 °C, while $Na_8Ti_5O_{14}$ is observed at 950 °C. $NaFeTiO_4$ and Na_2TiO_3 tend to reduce as the temperature increases, while $Na_{0.75}Fe_{0.75}Ti_{0.25}O_2$ increases with temperature (see Figure 12). Na_2TiO_3 reduction is believed to be due to a further reaction (combination) with $NaFeO_2$ to form of $Na_{0.75}Fe_{0.75}Ti_{0.25}O_2$ or similar phases with high utilisation of alkali, according to reaction (5):

$$3NaFeO_2 + Na_2TiO_3 \rightarrow 4Na_{0.75}Fe_{0.75}Ti_{0.25}O_2 + Na_2O \quad (5)$$

$NaFeTiO_4$ and $Na_2Fe_2Ti_3O_{10}$ were sporadically observed. $NaFeTiO_4$ was present at 550 ^oC and at 750 ^oC and above (see Figure 12). This phase is consistent with a 1:1 $FeTiO_3$:NaOH mole ratio. $Na_2Fe_2Ti_3O_{10}$ was only observed at 800 ^oC (seeFigure 10). Figure 12was obtained using the weight percent phase calculations as described in section 3.1.1.

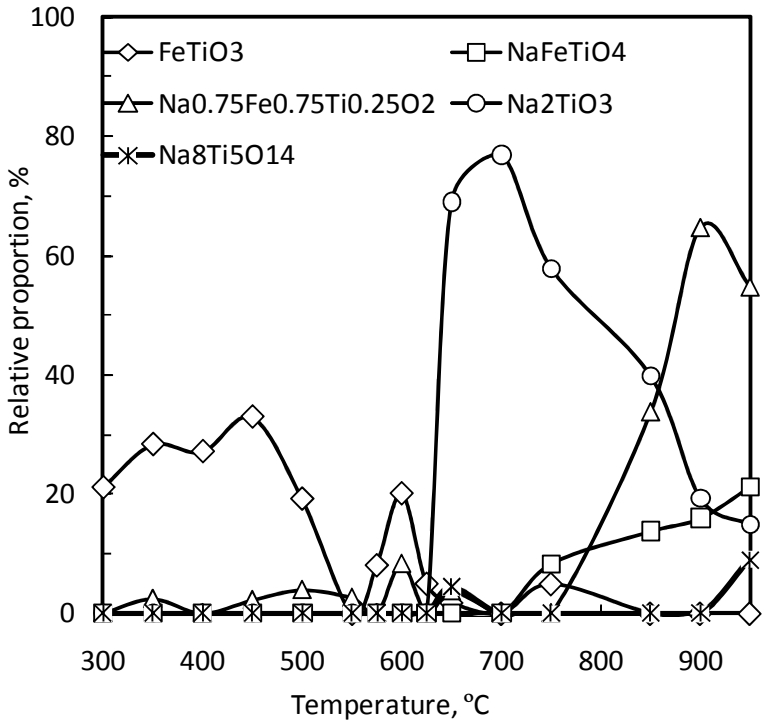

Figure 12: Phase correlation in the alkali fusion products, from the XRD semiquantitative weight percent. Samples were obtained by fusing the ore with NaOH (2:1 mole ratio) for 1 h

4.3.3 Effect of mole ratio and time

The effect of mole ratio was investigated at 750 ^oC using 2:1, 4:1 and 6:1 mole ratios ($NaOH:FeTiO_3$). The effect of time was tested at 30, 60 and 120 min of fusion. Table 8 shows the identified phases in the XRD analysis of alkali fusion decomposed ilmenite. The respective XRD diagrams are presented in Appendix A20–A28. Four titanium phases were identified in the

AFDI, namely $NaFeTiO_4$, $NaTiO_2$, $Na_8Ti_5O_{14}$ and Na_2TiO_3. Iron was chiefly accommodated in $NaFeO_2$.

Table 8: Identified phases by XRD in the AFDI diagrams obtained after roasting a mixture of ilmenite with sodium hydroxide for 1 h

Mole ratio, $NaOH:FeTiO_3$									
	2:1			**4:1**			**6:1**		
Time, min	30	60	120	30	60	120	30	60	120
$FeTiO_3$	minor	-	-	minor	-	-	minor	-	-
$NaFeTiO_4$	-	minor	major						
$NaTiO_2$	minor	minor	-	major	major	major	major	major	minor
$Na_8Ti_5O_{14}$	major	minor	-	minor	major	-	-	-	-
Na_2TiO_3	major	major	-	major	major	major	major	major	major
$Na_{0.75}Fe_{0.75}Ti_{0.25}O_2$	-	major	major	-	-	-	-	-	-
$NaFeO_2$	major	major	major	major	major	major	major	major	-
Na_2CO_3	trace	minor	-	major	trace	minor	major	major	-

Short periods of fusion produced mainly single titanates, irrespective of the mole ratio applied. At this temperature, fusions for a period of 30 and 60 min produced Na_2TiO_3 and $Na_8Ti_5O_{14}$. $Na_8Ti_5O_{14}$ was observed when two and four moles of NaOH were used, with a fusion period of up to 1 h. High mole ratios and extended periods of fusion did not favour $Na_8Ti_5O_{14}$. This was observed previously and was found to be consistent with the findings that this $Na_8Ti_5O_{14}$ is an intermediate in the roasting reaction (Batygin, 1967; Belyaev *et al.*, 1970; Belyaev, 1976).

At 2 h, at a mole ratio of 2:1 ($NaOH:FeTiO_3$), $NaFeTiO_4$ was the major phase. The existence of $NaFeO_2$ can be regarded as being a result of the reaction of Fe_2O_3 with NaOH, as was explained earlier. However, the relative amount in this case indicates that ilmenite was the source of iron. In fact, the major titanium phases are ternary ones.

4.3.4 Fusions under NaOH starved[10] conditions

Fusions under substoichiometric conditions were conducted in an effort to maximize the production of ternary phases. Those were considered as the most effective in recovering more titanium using the less amount of sodium hydroxide. Three mole ratios were analysed, namely 1:1, 1:2 and 1:4 ($NaOH:FeTiO_3$), at 550 and 850 ^oC fusion temperatures for 1 h. The identified phases in the XRD patterns are presented in Table. Under prevalent conditions, temperature is the determining factor. As is obvious from the results in Table, at 550 °C binary phases dominate (Na_2TiO_3 and $NaFeO_2$); while at 850 °C ternary phases dominate ($NaFeTiO_4$ and $Na_3Fe_3TiO_8$). At 550 ^oC, $FeTiO_3$ was the dominant phase irrespective of the mole ratio. At 850 ^oC $FeTiO_3$ was not observed in the products.

Table 9: Fusions of NaOH:Ilmenite ore under starving conditions for 1 h

	Temperature					
	550 °C			**850 °C**		
Mole ratio, $NaOH:FeTiO_3$	**1:4**	**1:2**	**1:1**	**1:4**	**1:2**	**1:1**
$FeTiO_3$	major	major	major	nd	nd	nd
$NaFeTiO_4$	nd	nd	nd	nd	minor	major
$NaTiO_2$	minor	nd	nd	nd	nd	nd
$Na_8Ti_5O_{14}$	minor	nd	nd	minor	nd	minor
Na_2TiO_3	minor	major	major	nd	nd	nd
$Na_3Fe_3TiO_8$	nd	nd	nd	major	major	major
$NaFeO_2$	major	major	major	nd	minor	minor

nd – non detected

At 550 ^{o} the principal titanium phase was Na_2TiO_3. $Na_8Ti_5O_{14}$ was present when a quarter of a mole of NaOH was used. Fe was accommodated chiefly in $NaFeO_2$. The phases obtained are improbable under the conditions used. Their formation indicates that the reaction did not proceed to its completion.

[10]Fusions using amounts of NaOH less than the stoichiometric amount

At 850 ^{o}C, $NaFeTiO_4$ and $Na_{0.75}Fe_{0.75}Ti_{0.25}O_2$ are the dominant phases. $Na_8Ti_5O_{14}$ and $NaFeO_2$ are present as minor phases. The former phases are non-equilibrium. The formation of $Na_8Ti_5O_{14}$ and $NaFeO_2$ has to be regarded as being kinetically driven. With longer fusion periods it is expected that $Na_8Ti_5O_{14}$ and $NaFeO_2$ will recombine and form ternary phases.

4.4 FT-IR Analysis

The fusion reaction was followed by infra-red spectroscopy. The spectra recorded at different fusion temperatures are presented in Figure 13. For AFDI samples obtained between 400 and 550 °C, a band at 3670–2350 cm^{-1} can be observed. This band can be attributed to different modes of O-H vibration in water (Ryskin, 1974). The presence of O-H bands indicates that NaOH did not react completely. These bands result from NaOH and from water absorbed by NaOH.

An overview of the region between 1800 and 400 cm^{-1} indicates the existence of two distinct regions: the first from 400–900 cm^{-1} and the second between 1300 and 1600 cm^{-1}, according to the disposition of the absorption bands in the spectra. Vibrations of ions in the crystal lattice are observed in the region of 1000–400 cm^{-1}, according to Sertkol *et al.* (2009).

In the first region (900–400 cm^{-1}), taking the ilmenite spectrum as the starting material, significant changes can be observed after NaOH addition with new bands at 630 and 900 cm^{-1}. The band at 900 cm^{-1} disappears above 550 ^{o}C, while the one at 630 cm^{-1} broadens with temperature.

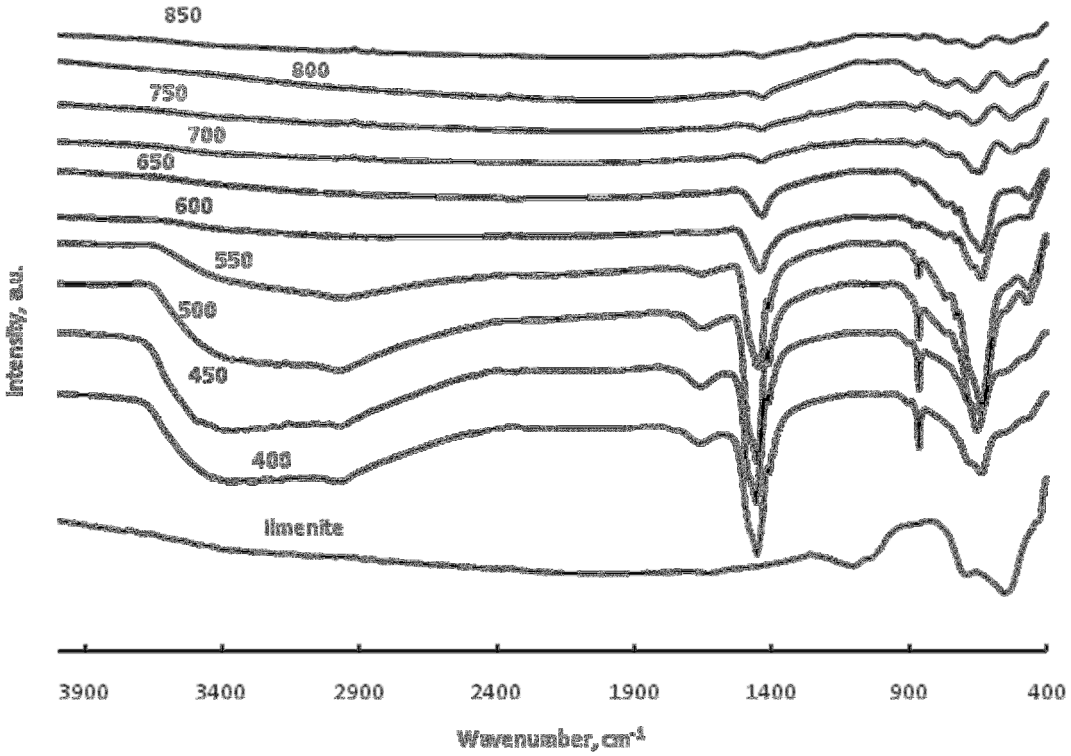

Figure 13:FT-IR spectra of alkali fusion decomposed ilmenite. Samples were obtained by fusing NaOH:$FeTiO_3$ mixtures (2:1 mole ratio) for 1 h at the indicated temperatures

In the 1600–1300 cm^{-1} region, AFDI at lower temperatures presents an absorption band from 1530–1340 cm^{-1}, with peaks at 1453, 1408 and a shoulder at 1484 cm^{-1}. This band weakens as the fusion temperature increases (see Figure 12).

The aim of the FT-IR analyses was to identify active groups at different fusion temperatures to elucidate the reaction mechanism. We looked into the evidence of formation of different groups. Under adequate conditions, temperature and mole ratios, the reaction of ilmenite (FeTiO3) with NaOH produces titanates and iron titanates. Ilmenite mineral ore, however, contains other chemical species present as impurities (see Table 4, Table 5 and Table 6).

Theexistence of such impurities, the mole ratio applied and the processing temperature can lead to different products, as can be seen in our results (see Table 7, Figure 10, and Table 8).

Iron silicates can be identified by a band in the region 930–1020 cm^{-1} (Jambor and Dutrizac, 1998). This band is observed in all AFDI samples. The band reduces intensity above 500 ^{o}C. It is an indication that iron silicates are part of the mechanism in earlier stages of the reactions. Above this temperature iron silicates apparently decompose. The XRD results show the existence of a sodium iron silicate ($Na_{0,925}Fe_{0.925}Si_{0.075}O_2$) phase at 500 ^{o}C (Appendix A-6; see Figure 14). This is important since it reduces sodium consumption, contributing to the economy of the process.

The presence of titanosilicates can be unequivocally established by the presence of bands at 960 and 1125 cm^{-1}, according to Ratnasamy *et al.* (2004). The peaks at around 1060 and 970 cm^{-1} are due to Si-O-Si asymmetric stretching in silicates (Muroya, 1999; Vicente-Rodríguez *et al.*, 1996).

Three groups of titanium structures are observed, according to our results: the TiO_4 tetrahedra, TiO_6 octahedra and TiO_5 groups. A band observed in all samples between 650 and 750 cm^{-1} is assigned to TiO_4 tetrahedra, while bands below or near 500 cm^{-1} are due to TiO_6 octahedra (Tarte *et al.*, 1979); these are also present in all samples. The TiO_5 group is present at 450, 500, 550, 600, 650, 700 and 850 ^{o}C (Figure 14 and Table 10). A band at 725 cm^{-1} is observed and is assigned to the TiO_5 group (Peng and Liu, 1995). The TiO_4 group is present in $M^{II}TiO_4$ compounds, the TiO_6 octahedra in sodium titanates and the TiO_5 group is present in Ti-O_x fresnoite-like ($Ba_2TiOSi_2O_7$) compounds (Gabelica-Robert and Tarte, 1981; Peng and Liu, 1995). Sodium iron titanates of the family $Na_xFe_xTi_{2-x}O_4$ are reported to have TiO_6 octahedra (Kuhn *et al.*, 1996). The ilmenite structure also possesses such groups. Pure TiO_2 presents an intense band between 900-450 cm^{-1} with a peak at 550 cm^{-1}.

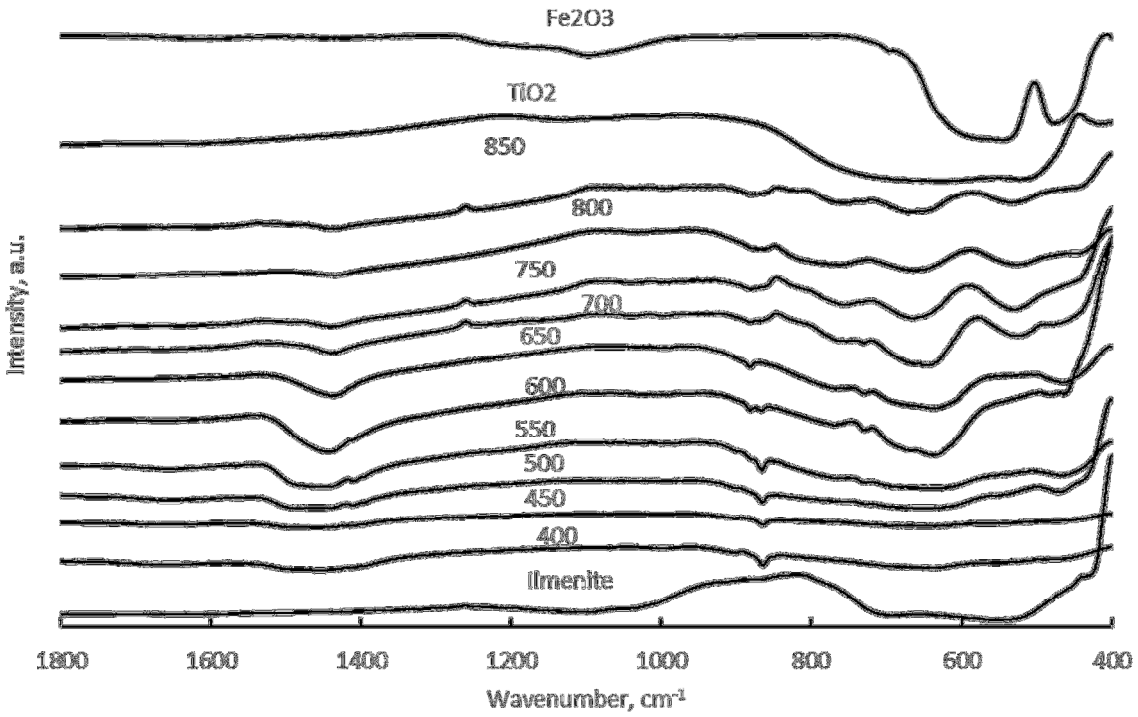

Figure 14: FT-IR spectra of the fusion-processed NaOH:$FeTiO_4$ mixtures (2:1 mole ratio), mid infra-red range. Samples were fused for 1 h at the indicated temperatures

Iron, as expected, is present in all samples. All samples exhibit maximum absorption in the region of 650–550 cm^{-1}. FeO_4 tetrahedra absorb in this region (Sertkol *et al.*, 2009; Tarte *et al.*, 1979). This is also observed in Fe_2O_3 spectrum, an intense absorption band is observed between 700-500 cm^{-1}. FeO_4 also absorbs in the region of 780 to 750 cm^{-1} (Licht *et al.*, 2005; Xu *et al.*, 2007). All samples present absorption bands in this region.The FT-IR assignments are summarised in Table 10.

Table 10: Assignments of FT-IR bands in ilmenite and fused products

Sample	Band position (cm^{-1})	Assignment	References
Below 600 °C	2400 and 3800	O – H stretching vibration in M – OH groups	Nagarajan and Rajendran, 2009 Ryskin, 1974
All	1600	Absorbed water	
All	1080	Si – O stretching in SiO_4 tetrahedral groups	Farmer, 1974; Méndez-Vivar *et al.*, 2001; Ratnasamy *et al.*, 2004
700 °C	1130	Ti – O in TiO_4 groups and MO – OM in terminal groups	Ratnasamy *et al.*, 2004
Below 800 °C	861	Ti – O stretching in TiO_6 Si – O symmetric vibration	Gabelica-Robert and Tarte, 1981
All	550–650	FeO_4 tetrahedral groups	Tarte *et al.*, 1979
450–700 °C	500	Ti – O stretching in TiO_6	Tarte *et al.*, 1979

4.5 Scanning Electron Microscopy

The ilmenite alkali fusion reaction was also studied by scanning electron microscopy (SEM). A panoramic view of the ilmenite ore SEM micrographs shows a random morphology of crystals (Figure 15(a)). In a closer look, the ilmenite crystals present lamellar aggregates (Figure 15(b)).

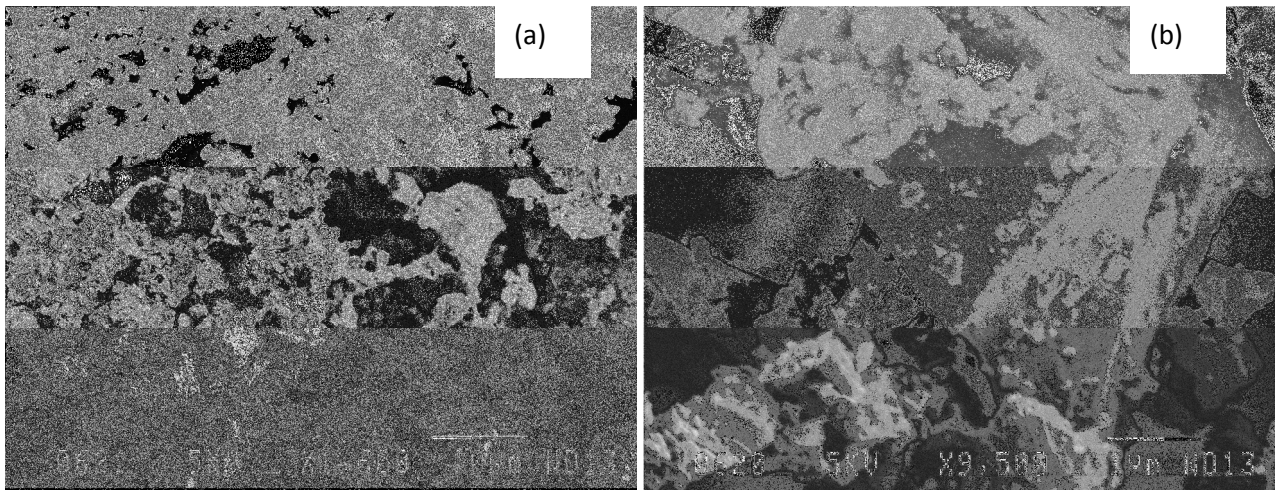

Figure 15: Microphotography of ilmenite ore material used in this study. (a) Lower magnification; (b) higher magnification

Variation in the crystal morphology during the reaction was identified by SEM. Figure 16shows ilmenite crystals (Figure 16(a)) collapsing to form a wafer-like morphology at 700 ^{o}C (Figure 16 (b)). As the fusion temperature increases, the wafer morphology is abandoned to assume a more disordered structure, a cotton seed-like morphology (Figure 16(c)), at 750 ^{o}C. A further increase in the fusion temperature, to 850 ^{o}C, resulted in the AFDI reacquiring the wafer-like morphology (Figure 16 (d)). This indicates the formation of ternary compounds by inclusion of sodium ions into the ilmenite crystal lattice.

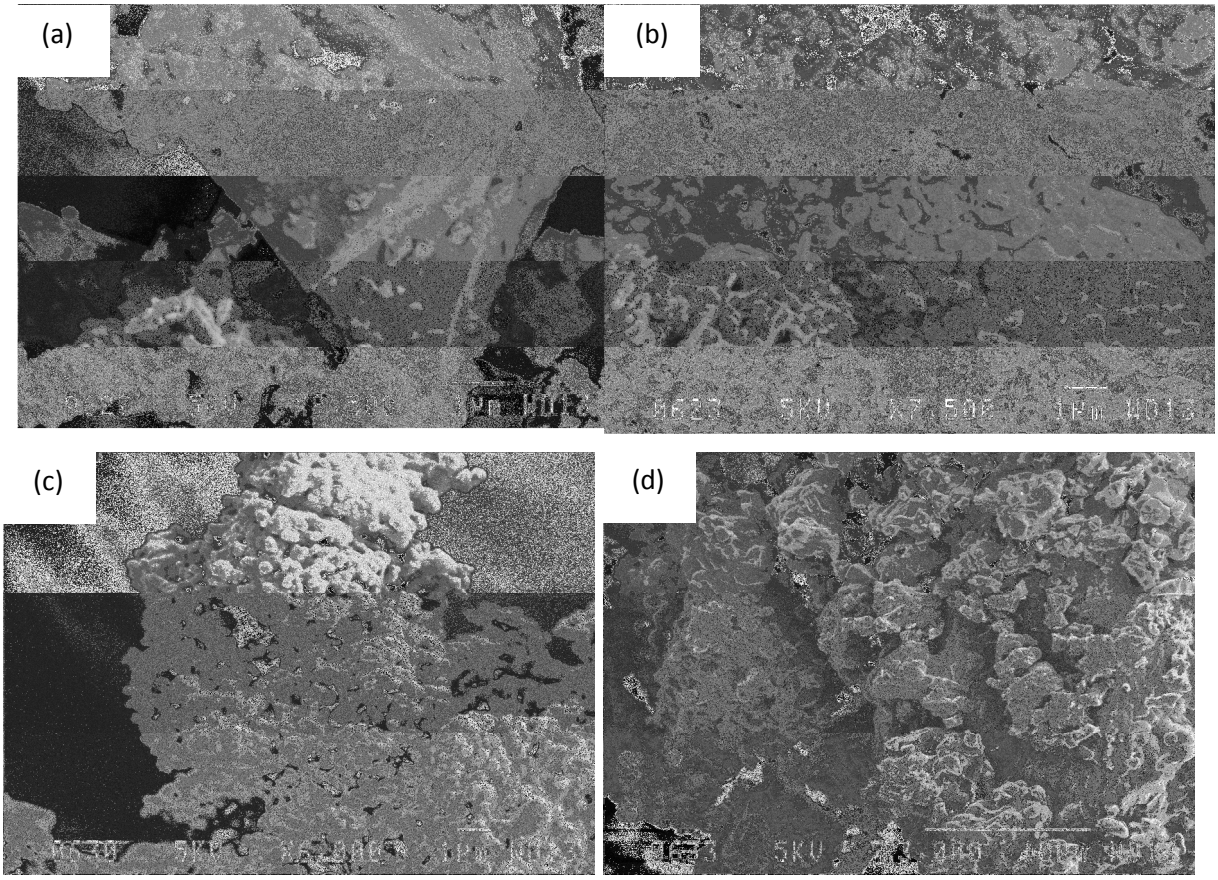

Figure 16: Microstructure evolution induced by the ilmenite alkali fusion reaction. (a) Ilmenite raw material; (b) NaOH:$FeTiO_3$ fused at 700 ^oC for 1 h; (c) NaOH:$FeTiO_3$ fused at 750 ^oC for 1 h; (d) NaOH:$FeTiO_3$ fused at 850 ^oC for 1 h

This reversibility of the crystal morphology was not observed in the colour of the crystals (Figure 17). The colour changes from black (ilmenite) to a maroon (850 ^oC). Intermediate AFDI samples present as green (500 ^oC) to a mixture of brown and green (650 ^oC).

Ferrous ion (Fe^{2+}) salts are green, while ferric ions (Fe^{3+}) are brown (or red). AFDI samples below 550 ^oC present a green colour, suggesting the predominance of iron in the ferrous oxidation state. This indicates that iron oxidises after being released from the ilmenite structure. In preliminary stages of the reaction, iron is released from the ilmenite structure. The

oxidation proceeds as the ilmenite structure is destroyed. Thus oxygen is the oxidant. Above 600 ^{o}C, iron oxidation to the ferric state is significant. The colour changes to red (brown).

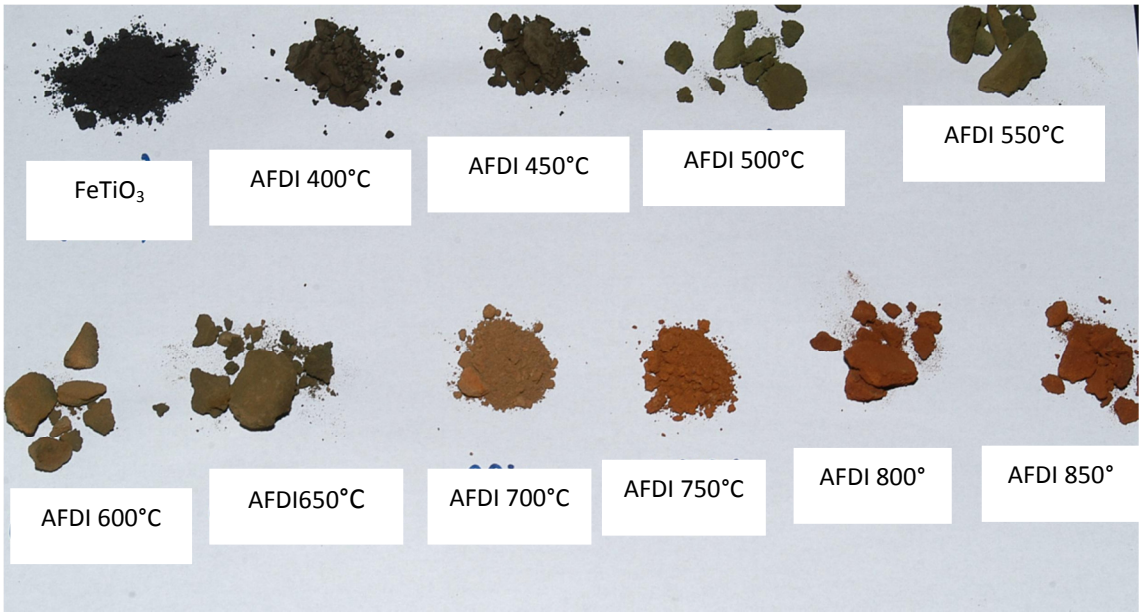

Figure 17: Colour evolution in ilmenite:NaOH mixtures (2:1 mole ratio) after fusion for 1 h at the indicated temperatures

4.6 Ilmenite Alkali Fusion Reaction

Five titanium-bearing phases were identified in our fusion products, namely $NaFeTiO_4$, $Na_8Ti_5O_{14}$, Na_2TiO_3, $Na_2Fe_2Ti_3O_{10}$ and $Na_{0.75}Fe_{0.75}Ti_{0.25}O_2$. The product spectrum is dependent on the mole ratio, temperature and time. Foley and Mackinnon (1970) also observed the dependency on the mole ratio.

At higher mole ratios, i.e. NaOH:$FeTiO_3$ equal to 4 or greater, alkali titanates and alkali ferrates are obtained. In this case the ilmenite structure is destroyed. Ti–O–Fe bonds are broken, forming Na–O–Fe and Na–O–Ti bonds. Ternary phases are not prevalent under these conditions. The reaction in this case is consistent with reaction equation (2) given in Section 4.3.1.

The results obtained show the presence of $Na_8Ti_5O_{14}$ as well. This can be explained by the observation made by Batygin (1967) on heating Na_2TiO_3, which can be assumed to be the following reaction (6):

$$5Na_2TiO_3 \rightarrow Na_8Ti_5O_{14} + Na_2O \quad (6)$$

$Na_8Ti_5O_{14}$ forms whenever there are insufficient sodium ions in the melt for the reaction to proceed. It is present when two or four moles of NaOH are used per mole of $FeTiO_3$. Its prevalence, however, reduces during prolonged fusion periods, as can be seen at 2 h (Table 8 and Figure 12).

Lower mole ratios combined with lower fusion temperatures or short periods of fusion produce similar results. This can be explained using melt viscosity and diffusion on the surface of the ilmenite crystals. As NaOH melts, it soaks the surface of the ilmenite crystals, dissolving them. The dissolved crystals are in an environment with a high concentration of sodium ions. This leads to a reaction in “artificial” mole ratio conditions. At lower fusion temperatures the melt viscosity is higher, which does allow the ions high mobility. The same results are observed when the fusion is conducted over short periods.

Mole ratios lower than 4:1 ($NaOH:FeTiO_3$), allied with high temperatures (above 550 ^oC) and fusion periods above 30 min, are conducive to the formation of ternary phases. It is worth noting that binary phases are also present. They accommodate the excess of either titanium (as titanates) or iron (as ferrates) upon the formation of the ternary phase (Foley and Mackinnon, 1970).

Alkali fusion of ilmenite is, however, better represented as sum of reactions (1) to (5). Depending on the parameters applied to the reaction, any of the products can be obtained.

Therefore the "net equation" will include all the observed phases in the product spectrum, and the proportions of each phase will be determined by the following parameters: temperature, time and mole ratio of the reactants. The following equation represents the net reaction (7).

$$28FeTiO_3 + 22Na_2O + 7O_2 \rightarrow 16Na_{0.75}Fe_{0.75}Ti_{0.25}O_2 + 3NaFeTiO_4 + 4Na_2Fe_2Ti_3O_{10} + 4Na_2TiO_3 + 2Na_8Ti_5O_{14} + 10NaFeO_2 \quad (7)$$

In fusions with 2:1 mole ratios ($NaOH:FeTiO_3$) at temperatures above 700 ^oC, $Na_{0.75}Fe_{0.75}Ti_{0.25}O_2$ is the dominant phase. This was also found by Foley and Mackinnon (1970) who indicated $Na_{0.75}Fe_{0.75}Ti_{0.25}O_2$ as the dominant phase when the ratio Na:Ti is equal to or above to 1:1. Simple titanates are also favoured under these conditions, due to the surplus titanium from $Na_{0.75}Fe_{0.75}Ti_{0.25}O_2$ (67% according to reacted Fe).

Other phases might be present, as indicated by other authors (Bayer and Hoffman, 1965; Foley and MacKinnon, 1970; Li *et al.*, 1971; Reid and Sienko, 1967), but they are beyond the detection limit of the method or else did not crystallise perfectly.

Based on our results, it is proposed that the reaction path proceeds according to the following mechanism:

- Initially, sodium ions, from NaOH melt, break the ilmenite lattice, producing titanates (Na_2TiO_3 mainly) and ferrates (mainly $NaFeO_2$).
- As the reaction proceeds and the concentration of Na^+ ions in the melt reduces, Na_2TiO_3 polymerises, favouring the reaction of Na^+ ions (reaction 2).
- Because Na^+ is proportionally insufficient to compensate for the demand for Ti^{4+} and Fe^{3+} ions in the event of the ilmenite lattice breaking, Na^+ ions are incorporated into the ilmenite lattice, resulting in the partial substitution of Ti^{4+} and Fe^{3+} ions in the lattice.

The SEM images indicate the regeneration of ilmenite crystal morphology as the reaction proceeds (Figure 16(a–d)), suggesting the incorporation of Na ions into the ilmenite lattice.

Silica impurities are trapped by sodium ions, forming sodium silicates. Titanium silicates are not formed, which could reduce the titanium yield. This was indicated by infra-red analyses.

4.7 Kinetics of the Ilmenite Alkali Fusion Reaction

4.7.1 Theoretical Background

Kinetic analyses provide information on the parameters of a chemical process. These parameters include the temperature (T) and the degree of conversion (α), essentially. The idea is to associate these reaction parameters with the rate equation ($f(\alpha)$), the pre-exponential factor (A) and the activation energy (E). This can be accomplished by thermal analysis. ICTAC[11] committee recommends the recommends a multiple heating rate program for computation of reliable kinetic parameters (Brown *et al.*, 2000; Vyazovkin *et al.*, 2011). The degree of conversion is obtain by the following equation

$$\boldsymbol{\alpha = \frac{w_0 - w}{w_0 - w_f}} \qquad \text{(Eq. 6)}$$

Where w_0 is the initial weight percent, w the actual weight and w_f the residual weight percent. The rate equation, in general, is a function of temperature and the degree of conversion according to the relation (Eq. 7)

$$\boldsymbol{\frac{d\alpha}{dt} = k(T)f(\alpha)} \qquad \text{(Eq. 7)}$$

Where K is the rate constant of the reaction. The rate constant gives the dependency of the process on the temperature. The influence of temperature on the constant rate is given by Arrhenius equation (Eq. 8)

[11] International Confederation for Thermal Analysis and Calorimetry

$$k(T) = A \exp\left(-\frac{E}{RT}\right) \quad \text{(Eq. 8)}$$

Where *A* is the pre-exponential factor, *E* is the activation energy and *R* is the universal gas constant. *A* and *E* are termed Arrhenius or kinetic parameters.

Combining Eq. 7 and Eq. 8 we obtain

$$\frac{d\alpha}{dt} = A \exp\left(-\frac{E}{RT}\right) f(\alpha) \quad \text{(Eq. 9)}$$

Eq. 9 is the basis of differential kinetic programs. In this form can be used to obtain all the kinetic parameters using any temperature program, isothermal or non-isothermal. A non-isothermal program will require a substitution of the actual temperature of the sample (Vyazovkin *et al*., 2011). This can be achieved by introducing the heating rate (β) in Eq. 9

$$\beta \frac{d\alpha}{dT} = A \exp\left(-\frac{E}{RT}\right) f(\alpha) \quad \text{(Eq. 10)}$$

The introduction of β in Eq. 10 implies that the sample has to follow exactly the heating program ideally. That means sample temperature as to be always equal to reference temperature. In most experimental cases there is a deviation from the reference temperature. This reduces the applicability of Eq. 10 (Vyazovkin *et al*., 2011; Lick *et al.,* 2012). Integration of Eq. 10 gives

$$g(\alpha) = \int \frac{d\alpha}{f(\alpha)} = \frac{A}{\beta} \int \exp\left(-\frac{E}{RT}\right) dT = \left(\frac{AE}{R\beta}\right) \int \exp \frac{(-x)dx}{x^2} = \left(\frac{AE}{R\beta}\right) p(x) \quad \text{(Eq. 11)}$$

g(α) is the integral form of the rate equation; *p(x)* is the temperature integral for *x* = E/RT. Eq. 11 contains the term β, as was indicated it reduces its applicability.

Isoconversional principle states that the reaction rate at constant degree of conversion is only function of temperature (Vyazovkin *et al*., 2011). These methods allow the determination of the activation energy without the assumption of a specific reaction rate model. The application of this method requires a series of curves recorded at different heating rates. There are a number of mathematical expressions used which differ on the approximations made on the temperature integral. The most common is the Kissinger-Akahira-Sonose equation (Vyazovkin *et al*., 2011)

$$\ln\left(\frac{\beta}{T_p^2}\right) = \ln\left(\frac{AR}{E\, g(\alpha)}\right) - \frac{E}{RT} \qquad \text{(Eq. 12)}$$

where T_p is maximum in the DTA or DTG curves. Plotting $\ln(\beta/T^2)$ versus 1/T the activation energy can be obtained from the slope of the curve. The isoconversional method is unable to calculate the pre-exponential factor and to determine the kinetic model of the rate reaction model (Vyazovkin, 2008).

The model-fitting or the Coats-Redfern allows the determination of the kinetic triplet, activation energy, pre-exponential factor and the kinetic model. In this approach the difference between measured and calculated data on the reaction rate is minimized. This minimization can be achieved by linear methods. According to ICTAC recommendation this procedure is reliable when multiple sets of data are fitted to the models (Vyazovkin *et al.*, 2011).

The mathematical expression used for model fitting can be derived from Eq. 12. Rearranging this equation (Eq. 12) it gives (Eq. 13) (Khawam and Flanagan, 2005; Lick *et al.,* 2012; Manikandan *et al*., 2011).

$$\ln\frac{g(\alpha)}{T^2} = \ln\left(\frac{AR}{\beta E}\left[1 - \left(\frac{2RT}{E}\right)\right]\right) - \frac{E}{RT} \qquad \text{(Eq. 13)}$$

Plotting ln[g(α)/T^2] versus 1/T using the correct $g(\alpha)$ function gives a straight line which slope gives E/R. The pre-exponential factor can be calculated from the obtained activation energy.

The most probable mechanism was further confirmed by using the master plot method. This method is more accurate and less influenced by experimental conditions (Criado, 1978; Criado *et al*., 1989; Jin *et al*., 2009). The master plot curve can be obtained by plotting the conversion degree α against z(α). The former can be calculated for a chosen pair of rate function by (Eq. 14)

$$z(\alpha) = f(\alpha) \times g(\alpha) \qquad \text{(Eq. 14)}$$

The most probable mechanism is the one best fitting the experimental results.

4.7.2 Kinetic Analysis of Alkali Fusion Reaction

To study the kinetic of the ilmenite alkali fusion reaction, we conducted TGA experiments using three different heating rates, namely 2, 5 and 10 ^{o}C/min. In order to avoid concurrent reactions from ilmenite ore impurities, analytical grade $FeTiO_3$ from Sigma Aldrich was used. Ilmenite was mixed with powdered NaOH in an agate mortar. The mixed sample was weighed and subjected to thermogravimetric analysis at. The TGA and DTG curves are presented in Figure 18.

No changes were observed bellow 100 °C in all heating rates. A smooth change in the shape of the TG curves with an increase in the heating rate is observed. Although the initial temperature of mass loss is clearly observable at 2 ^{o}C/min, at 10 ^{o}C/min that point is difficult to determine. Above 400 °C the TGA signal, in Figure, shows a mass gain in the reaction. The DTA curves, as well as the DTG curves (in Figure 18), indicate an increase in T_{max} with heating rate (Table 11).

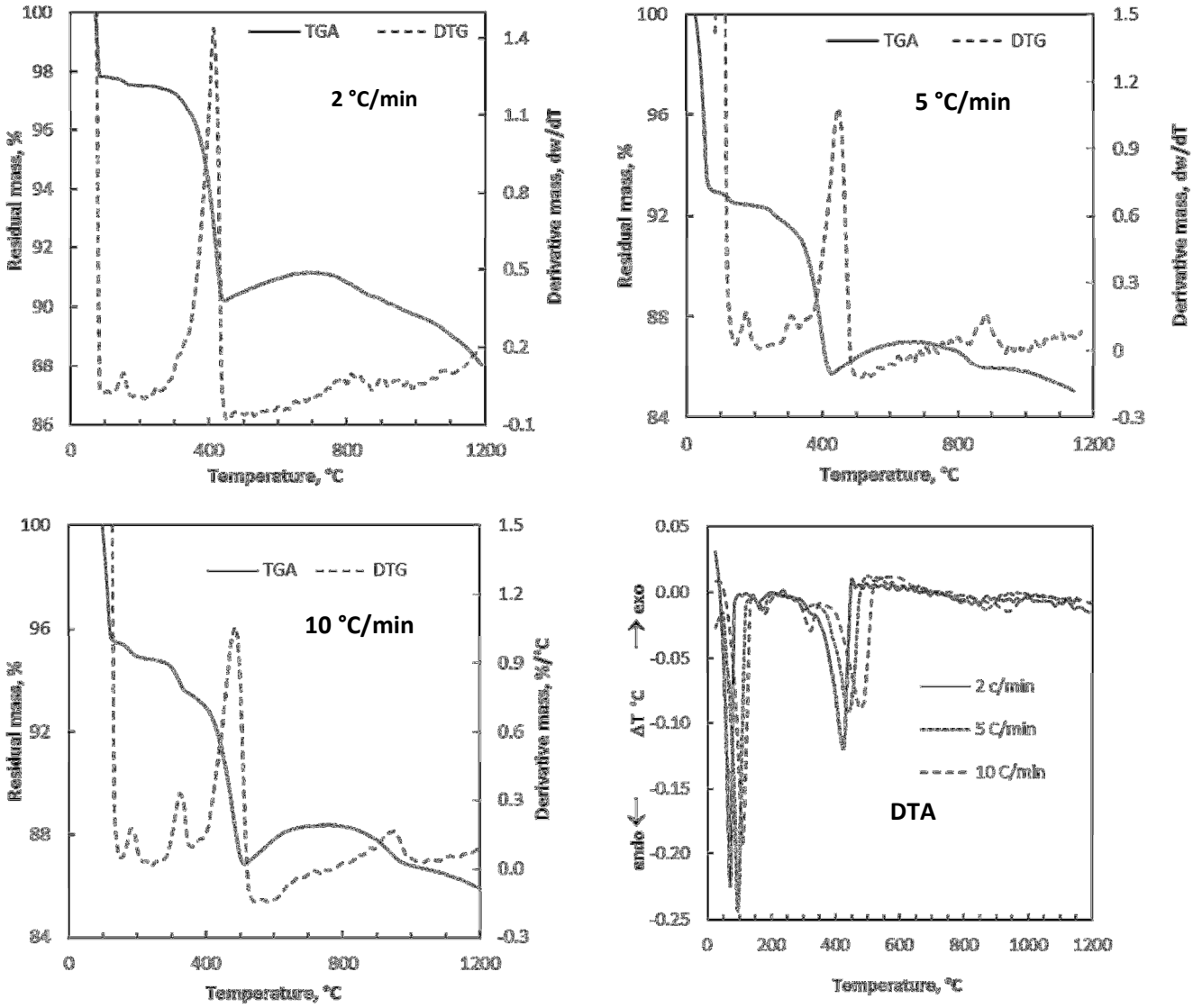

Figure 18: TGA, DTG and DTA curves of the ilmenite alkali fusion reaction at three different heating rates, 2, 5 and 10 °C/min

Table 11: Characteristics of TGA and DTA results of the ilmenite alkali fusion reaction

Heating rate (°C/min)	T_i (°C)	T_f (°C)	T_{max} (°C)	Mass loss (%)
2	155	449	425.5	7.449
5	143	424	448.2	3.948
10	193	512	488.6	8.001

T_i= initial temperature; T_f= final temperature; T_{max} = temperature at the maximum reaction rate

It was expected that mass loss would diminish with increasing heating rate. The highest mass loss was recorded at 10 °C/min. This is certainly due to the overlapping of moisture release and water released due to the reaction itself. DTG and DTA curves at the former heating rate (10 °C/min) show the appearance of a new maximum at 323 °C, see Figure 19. Apparently there is another endothermic reaction taking place at this temperature.

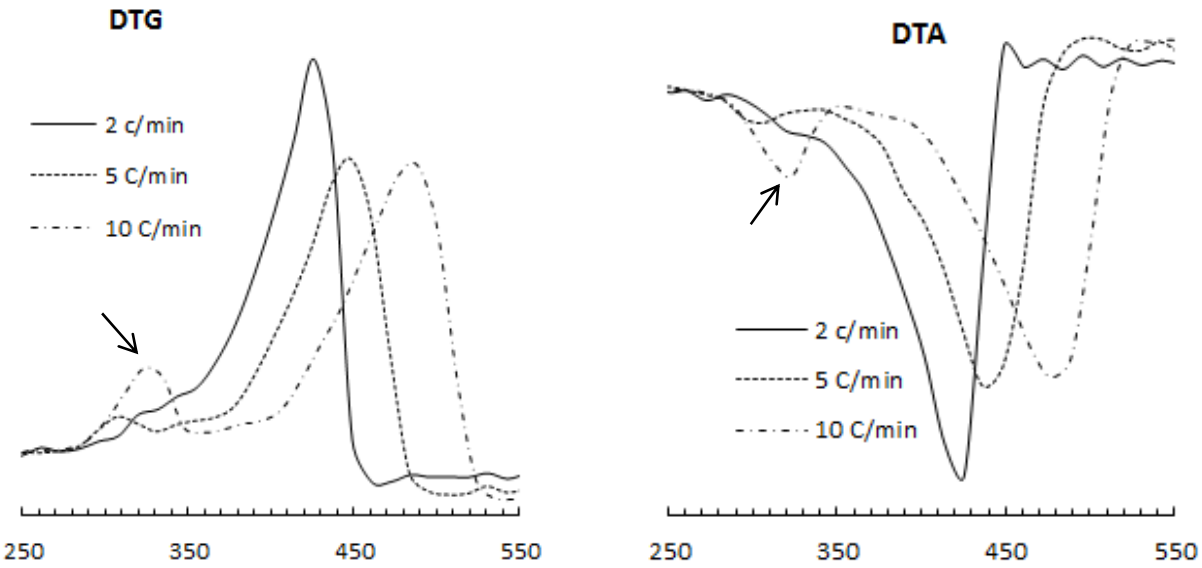

Figure 19: Section of the DTG and DTA signal displaying the new maximum

Based on Figure 19 and Figure 20 it is clear that there are at least two different reactions occurring. This makes it very difficult to fit kinetic models to the data, especially considering the fact that reaction occurring below 350 °C is accentuated as the temperature scan rate is increased. The simplistic models listed in Table 12 are unable to account for such effects.

For simpler kinetic behaviours the Dollimore procedure could be used to estimate the most probable mechanism. See Table for common models. Unfortunately that was not possible for the present data set (Chowlu *et al.*, 2009; Dollimore*et al.*, 1996; Jin *et al.*, 2009).

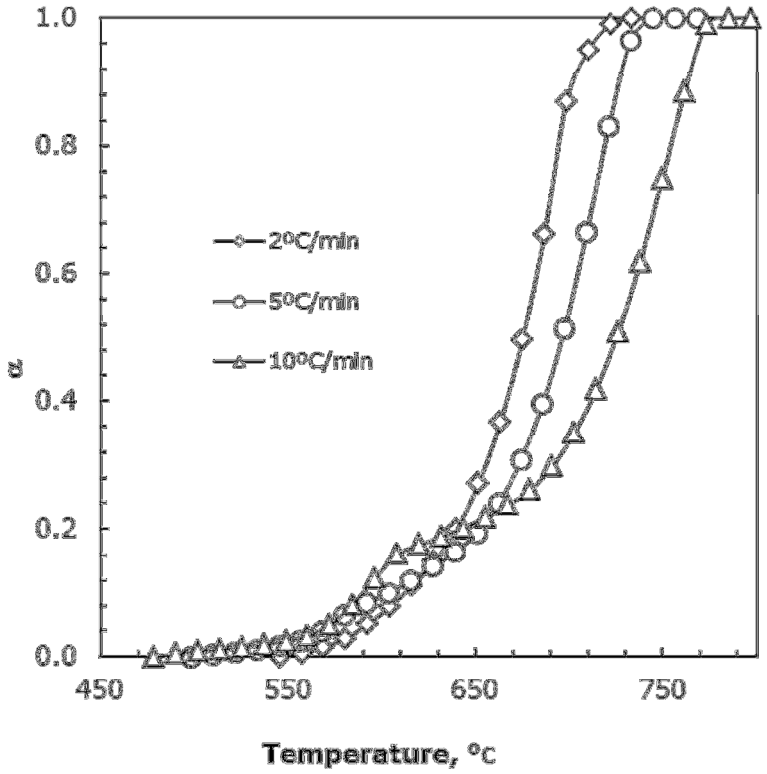

Figure 20: Conversion (α) as function of temperature in the alkali fusion reaction of ilmenite

However, it is clear that the reaction occurring at the higher temperature is the dominant one. Figure 20 shows that it accounts for more than 75% of the conversion. The activation energy for this reaction step can be estimated using the Kissinger method (Khawam and Flanagan, 2006). The basic assumption here is that this step can be described by n^{th} order reaction. In that case the activation energy is given by the slope of the plot of $\ln(\beta/T_p^2)$ versus $1/T_p$.

$$\ln\frac{\beta}{T_p^2} = \ln\left(\frac{AR\left(n(1-\alpha)_p^{n-1}\right)}{E_a}\right) - \frac{E_a}{RT_p} \qquad \text{(Eq. 15)}$$

Where T_p is the temperature of the maximum rate of conversion. Figure 21 shows the results of such an analysis. It is clear that the dada points do not fall on straight line. The implication is that the kinetics of the alkali fusion reaction cannot be modelled in such simple terms.

Table 12: Selected mathematical functions of the reaction mechanisms tested with produced data

Model	**Differential form** $f(\alpha)=\frac{1}{k}\frac{d\alpha}{dt}$	**Integral form** g(α)
Geometrical contraction models		
Contracting area (R2)	$2(1-\alpha)^{1/2}$	$[-(1-\alpha)^{1/2}]$
Contracting volume (R3)	$3(1-\alpha)^{2/3}$	$[-(1-\alpha)^{1/3}]$
Diffusion models		
1D Diffusion (D1)	$1/2\alpha$	α^2
2D Diffusion (D2)	$[-\ln(1-\alpha)]^{-1}$	$[(1-\alpha)\ln(1-\alpha)]+\alpha$
3D Diffusion – Jander Eq. (D3)	$3(1-\alpha)^{2/3}/2(1-(1-\alpha)^{1/3})$	$[1-(1-\alpha)^{1/3}]^2$
Ginstling-Brounshtein (D4)	$(3/2((1-\alpha)^{-1/3}-1)$	$1-(2\alpha/3)-(1-\alpha)^{2/3}$

Geometric models take into account systematic variations in the total area of the reaction interface. These variations are due to continuous change in geometry resulting from the advance of the reaction. Diffusion models consider that the rate determining step is the mass transport through product layer (Harrison, 1969).

The Jander equation and the Ginstling-Brounshtein equation are used in the case of advancing reaction interface. The Jander equation presents a rough approximation and should be used only for small extents of conversion ($\alpha = 0.15$). The Jander equation considers the convergence of the diffusion paths as the centre of the sphere is approached (Harrison, 1969).

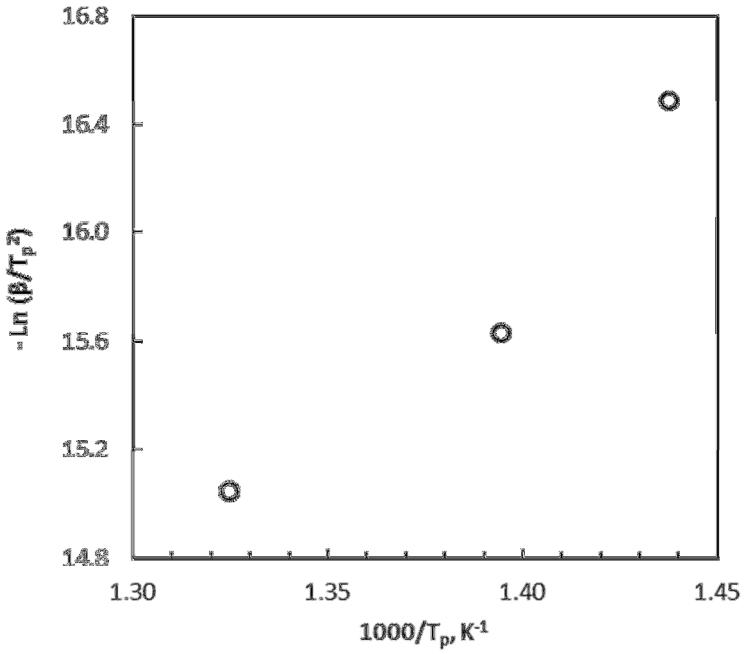

Figure 21: Kissinger plot for the dominant alkali fusion reaction

4.8 Optimisation of the Fusion Process

4.8.1 Effect of particle size

The effect of particle size was tested using an extreme particle size difference, $d_{50} \approx 6$ and 139 µm. Fusions were conducted at 550 to 900 ^{o}C (in 50 ^{o}C increments) for 1 h at a 2:1 mole ratio ($FeTiO_3$:NaOH). The results are presented in Figure 22 (a–c).

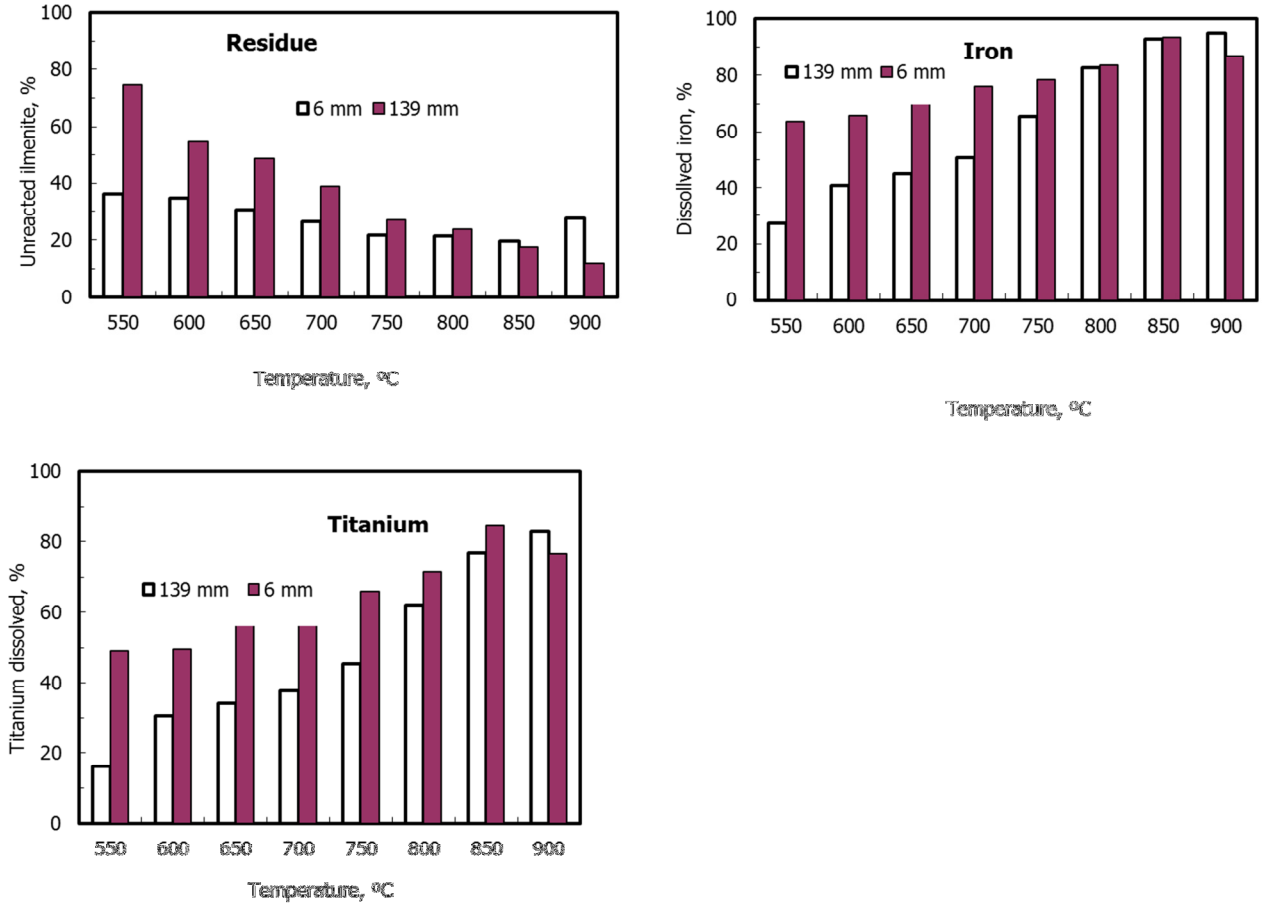

Figure 22: Effect of particle size. (a) Residue; (b) iron; (c) titanium[12]

At lower temperatures the coarser ilmenite produces, comparatively, high amounts of residue. At high temperatures this difference disappears. Such behaviour reinforces the finding of a diffusion-controlled reaction mechanism.

The comparatively higher amount of residue observed at 850 and 900 ^{o}C with finer ilmenite must be considered to be a result of agglomeration, which prevented part of the ilmenite from reacting. Higher temperatures lead to internal structure porosity breackdown (Johansson, 2007). Leion *et al*. (2008) reported the oxidation of ilmenite to Fe_2TiO_5 + TiO_2, around this temperature.

[12] mm stands for µm

4.8.2 Effect of mole ratio

Figure 23 indicates a steady increase in the amount of dissolved iron from 1:1 up to 2:1 ($NaOH:FeTiO_3$). High alkali recoveries are achieved when high quantities of NaOH per mole of ilmenite are used. Binary phases are predominant which are promptly hydrolysed in water, as shown in Figure 12. Around 96% are recovered when six moles of NaOH are used per mole of $FeTiO_3$. A temperature of 850 ^{o}C was used in an attempt to produce ternary phases, sodium iron titanates, especially when fusing below a 2:1 mole ratio (Lasheen, 2008). This was also confirmed in this work (Figure 12).

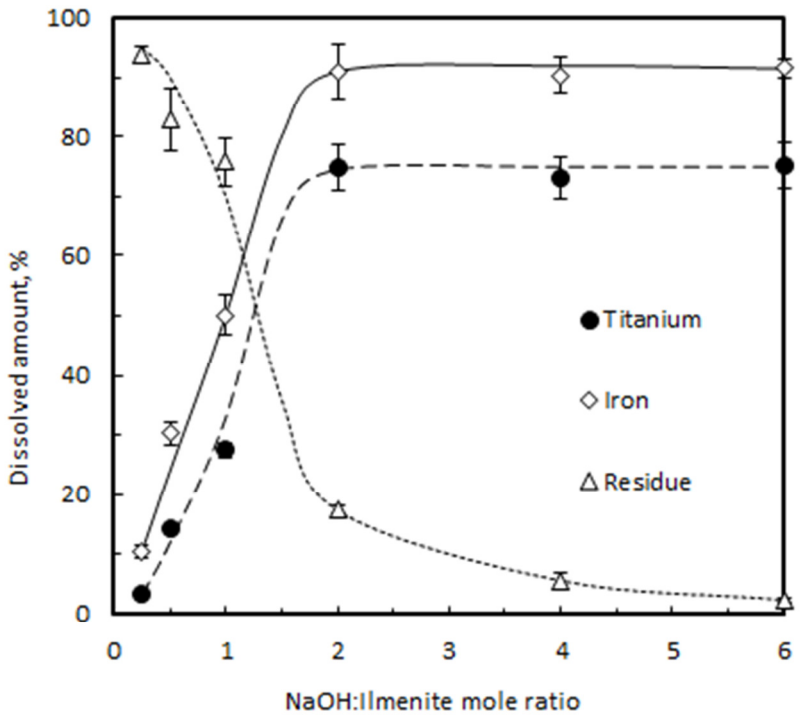

Figure 23: Effect of mole ratio on fusions conducted at 850 ^{o}C for 1 h

4.8.3 Effect of time

The effect of time in the fusion process was studied at 750 °C. Fusions were conducted 30, 60, 90, 120, 150 and 180 min, using two moles of NaOH per mole of $FeTiO_3$. The results are presented in Figure 24.

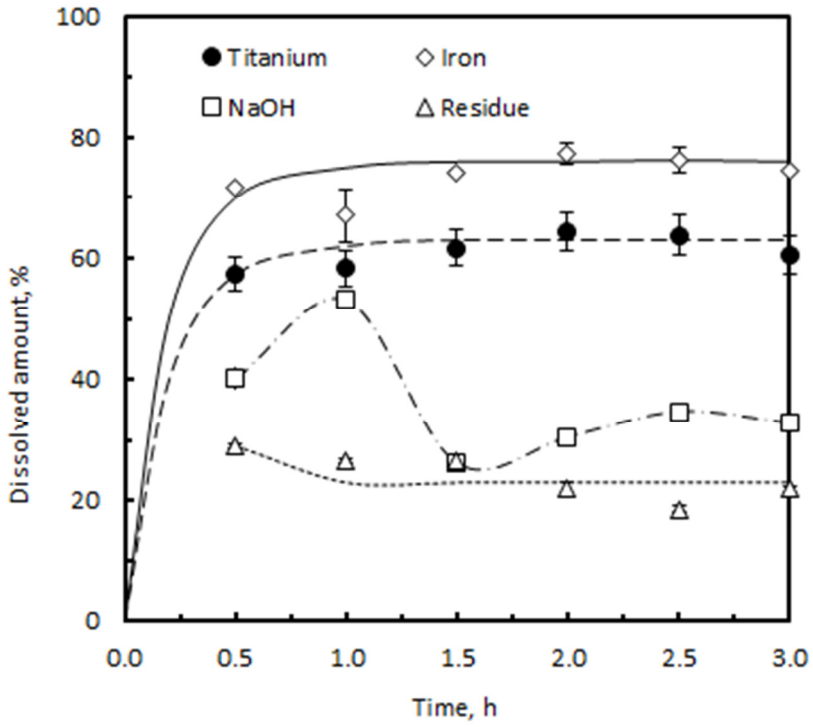

Figure 24: Effect of fusion time on the ilmenite alkali reaction (2:1 NaOH:$FeTiO_3$ mole ratio, 750 °C)

A plateau is observed after 1 h of fusion, meaning that extended periods of fusion do not increase the amount of species dissolved. In other words, under prevailing conditions the reaction between NaOH and $FeTiO_3$ is completed after 1 h. The alkali recovery reduces with time due to the formation of less hydrolysable species, supposedly ternary phases. The XRD results showed an increase in $NaFeTiO_4$ content with time of fusion (see Figure 24).

4.8.4 Effect of temperature

The effect of temperature was investigated using two moles of NaOH per mole of $FeTiO_3$ for 1 h of fusion in the 300 to 950 ^{o}C temperature range, gradient 50 ^{o}C. The results are presented in Figure 25.

Our results indicate a steady increase in the yields between 400 and 900 ^{o}C. A maximum is achieved closer to the 900 ^{o}C point, with 95% for iron and 81% for titanium. Above the 900 ^{o}C point, the solubilised amount of titanium and iron decreased.

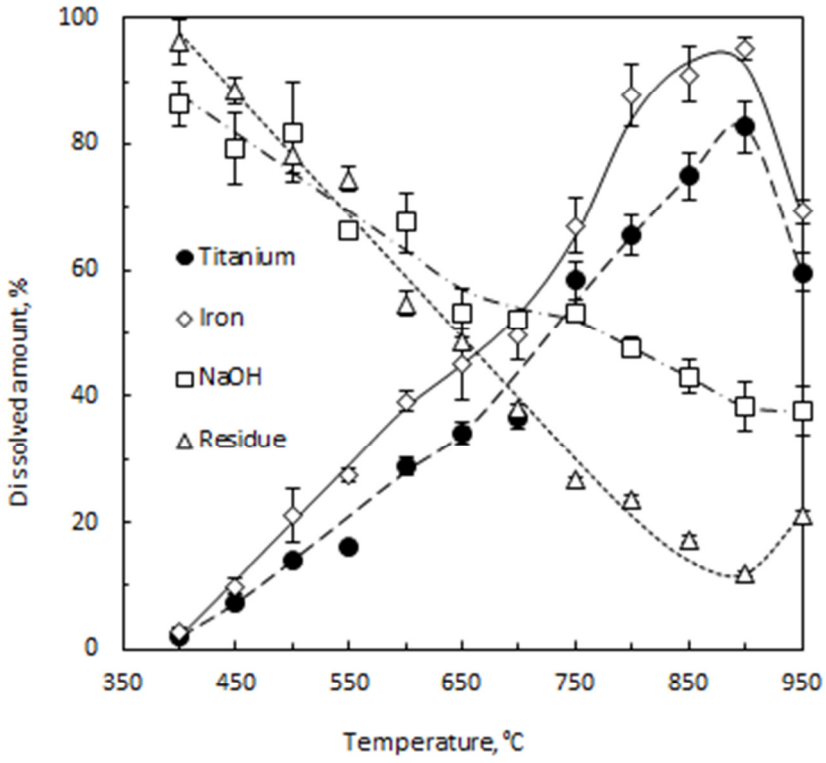

Figure 25: Effect of fusion temperature on titania recovery

The residue curve decreases steadily up to 900 ^{o}C where it reaches its minimum, 19%. This is in accordance with the iron and titanium solubilisation curve. Meanwhile the alkali recovery curve

shows a reduction in recoverable alkali. This is an indication of the formation of species that are not easily hydrolysable at high temperature. Higher levels of ternary phases were observed at this temperature from the XRD results, with $Na_{0.75}Fe_{0.75}Ti_{0.25}O_2$ being the main phase, as indicated in Figure 12.

4.9 Reagent Consumption

The efficiency of the process was investigated by comparing the titania yield against the amount of sodium hydroxide consumed (mass per mass basis), using six mole ratios (1:4, 1:2, 1:1, 2:1, 4:1 and 6:1 NaOH:$FeTiO_3$) for 1 h of fusion. The results are presented in Figure 26. The highest efficiency was attained using two moles of sodium hydroxide at 850 ^{o}C. Approximately 0.41 units are liberated per unit mass of NaOH. The theoretical maximum for this point is 0.53.

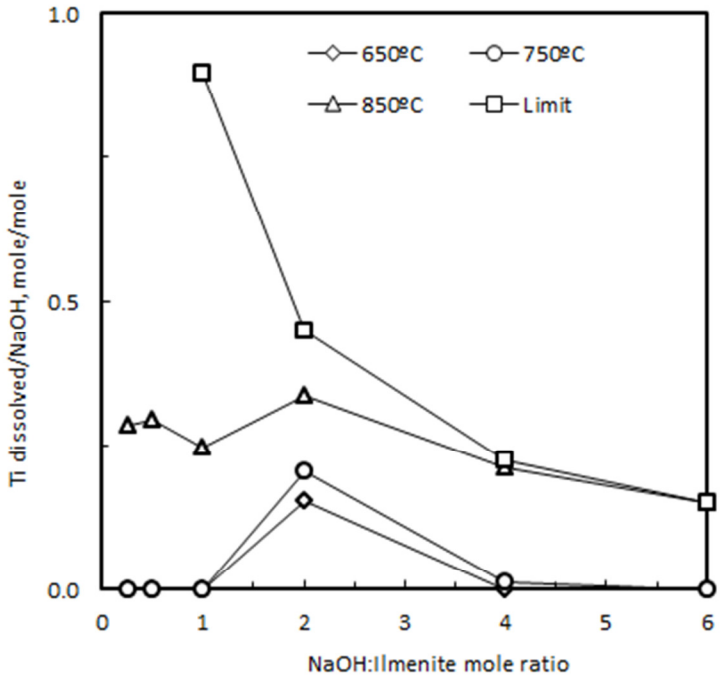

Figure 26: Efficiency of the fusion process

4.10 Optimisation of the Leaching Process

4.10.1 Effect of solid:liquid ratio

The effect of the solid:liquid (S:L) ratio was investigated at room temperature, using AFDI prepared by fusing two moles of NaOH per mole of $FeTiO_3$ at 750 ^{o}C for 1 h. Three ratios were tested, namely 0.20, 0.26 and 0.39, corresponding respectively to 200, 150 and 100 mL of distilled water per 30.35 g of ilmenite ore and a corresponding mass of NaOH. The results obtained are presented in Figure 27. Results are presented in terms of alkali recovered and determined by titration with HCl. This is the alkali that can be recycled.

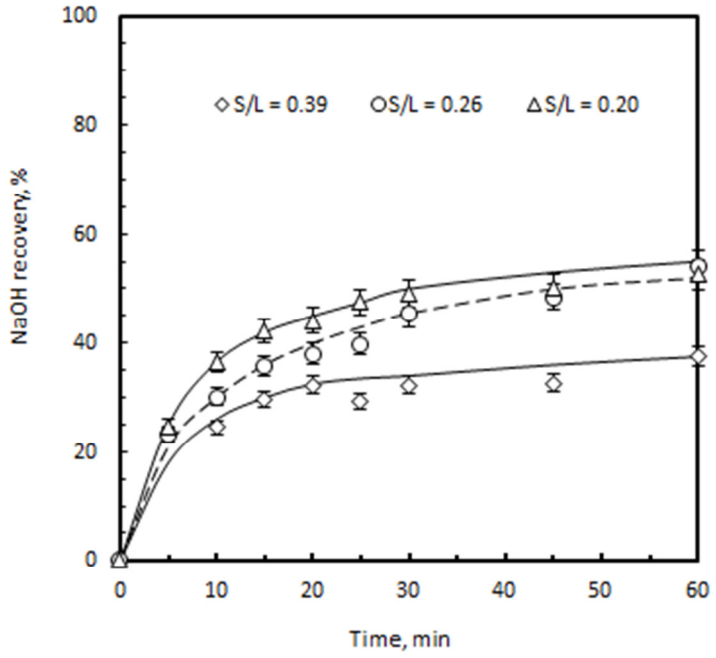

Figure 27: Effect of solid:liquid ratio on the leaching process at room temperature. Samples of AFDI were prepared by fusing two moles of NaOH with one mole of $FeTiO_3$ for 1 h at 750 ^{o}C

Our results indicate that S:L = 0.20 presents optimal extraction conditions. A maximum of 54% was obtained after 1 h of leaching, with 50% extracted after 30 min. In the first 5 min, no difference in terms of the amount of alkali extracted was observed.

4.10.2 Effect of time and temperature

The effect of time and temperature on the leaching process was investigated at intervals of 10 to 60 min at room temperature, 35, 40, 50 and 75 ^{o}C, using AFDI obtained by fusing a mixture of two moles of NaOH per mole of $FeTiO_3$ for 1 h at 750 ^{o}C. The solid:liquid ratio (S:L ≈ 0.26) was kept constant. The results are presented in Figure 28.

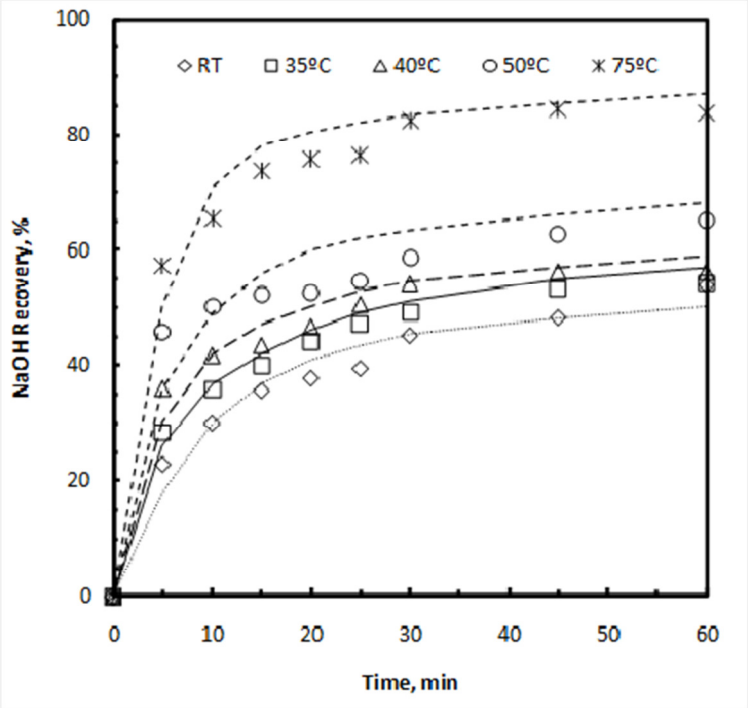

Figure 28: Effect of time and temperature on the leaching process. Samples of AFDI were prepared by fusing two moles of NaOH with one mole of $FeTiO_3$ for 1 h at 750^{o}C

In general, alkali recovery increases sharply up to 15 min. Above 15 min the rate of extraction does not increase. Approximately 75% of the total NaOH was extracted after 15 min of leaching at 75 ^{o}C, while at room temperature only 40% had been extracted after the same leaching time. The existence of phases that hydrolyse only at high temperatures is the rational explanation for the significant difference.

4.10.3 Batch leaching

The significance of repeated leaching was tested by repeating the leaching process three times, 5, 10 and 15 min for each leaching. The results are presented in Figure 29.

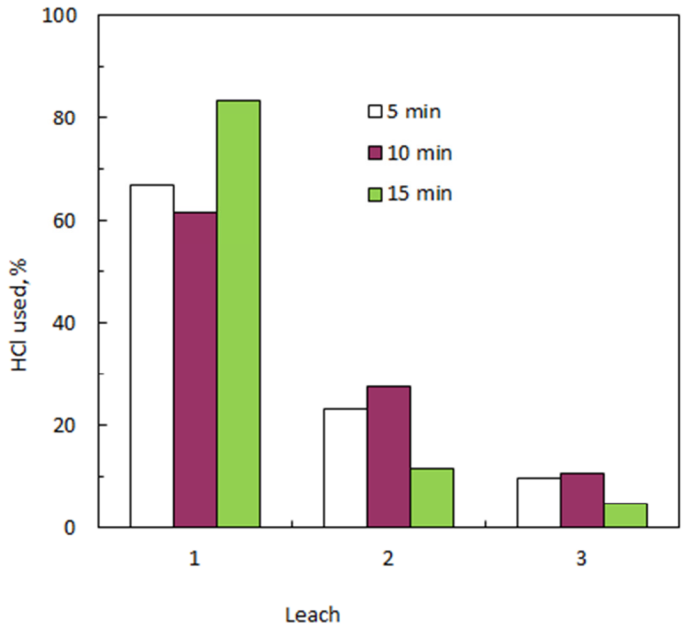

Figure 29: Effect of repeated leaching at indicated leaching times (batch leaching)

According to our results, a single leach can remove up to 83% (15 min leaching) of the total of recoverable alkali. Leaching tests were conducted at room temperature.

4.10.4 Kinetics of the leaching process

During leaching alkali fusion products are hydrolysed and sodium hydroxide used in the fusion process is recovered. The reactions occurring during hydrolysis can be summarised as follows, according to the net equation (7) presented before:

$$Na_2TiO_3 + 2H_2O \rightarrow 2NaOH + TiO(OH)_2$$

$$Na_8Ti_5O_{14} + 9H_2O \rightarrow 8NaOH + 5TiO(OH)_2$$

$$NaFeO_2 + H_2O \rightarrow NaOH + FeOOH$$

For practical purposes it was assumed that only one of the above reactions is occurring, the reaction of $NaFeO_2$ was considered as the most probable to occur under the considered fusion conditions. Ternary phases are stable to aqueous hydrolysis. These phases hydrolyse under acidic conditions, as was reported by Foley and MacKinnon (1970).

The experimental data were fitted to leaching models in order to determine the rate-controlling step and kinetic parameters. According to Demirkiran (2008), these processes are controlled either by diffusion through the fluid film, diffusion through the product layer, or by the chemical reaction at the surface. The mathematical expressions of such models are (Eq. 16):

$$1 - (1 - \alpha)^{\frac{1}{3}} = \frac{K_C MC}{\rho a r_0} t = k_r t \qquad \text{(Eq. 16)}$$

for the surface chemical reaction and (Eq. 17):

$$1 - \frac{2}{3}\alpha - (1 - \alpha)^{\frac{2}{3}} = \frac{2MDC}{\rho a r_0} t = k_d t \qquad \text{(Eq. 17)}$$

for the diffusion-controlled reaction.

where α is the reacted fraction, M is the molecular mass of the solid, C is the concentration of the leachant in the solution, ρ is the density of the solid, a is the stoichiometric coefficient of the leaching reaction, r_0 is the initial radius of the solid particle, D is the diffusion coefficient in the product layer, t is time, and K_r and K_d are the rate constants for the reaction.

In some cases the leaching process can be controlled by a mixed mechanism. In this case the two mathematical expressions are combined, resulting in the following equation (18) (Dehgan *et al*., 2009):

$$\left[1-(1-\alpha)^{\frac{1}{3}}\right]+B\left[1-\frac{2}{3}\alpha-(1-\alpha)^{\frac{2}{3}}\right]=kt \qquad \text{(Eq. 18)}$$

Where$B=K_r/K_d$ and K are the rate constants of the mixed mechanism.

Dickinson and Heal (1999) suggested a new equation for a shrinking core mechanism during leaching (Eq. 19). Dehghan *et al.* (2009) used the same model for experimental data of sphalerite leaching with HCl-$FeCl_3$.

$$\frac{1}{3}\ln(1-\alpha)+\left[(1-\alpha)^{-\frac{1}{3}}-1\right]=kt \qquad \text{(Eq. 19)}$$

Our experimental data, however, did not fit any of the above proposed models. Figure 30 shows the degree of conversion versus time obtained from our experimental data.

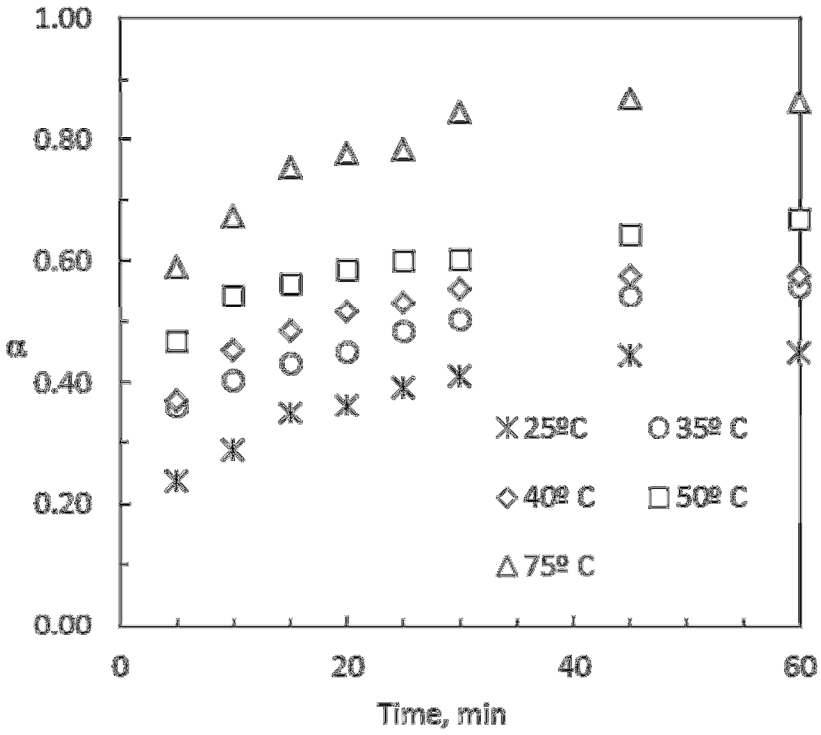

Figure 30: Plot of leaching kinetics

4.11 Optimal Hydrolysis pH

The optimal hydrolysis pH was determined by varying the final pH from 2 to 7 (0.5 intervals) and determining the relative amount of iron and titanium in the solution. The results are presented in Figure 31.

According to our results, the pH value is not significant above 3. Less than 1% of titanium and iron is dissolved above that point, for both titanium and iron. Based on that, a pH of 7 is recommended since it will require less acid consumption for hydrolysis.

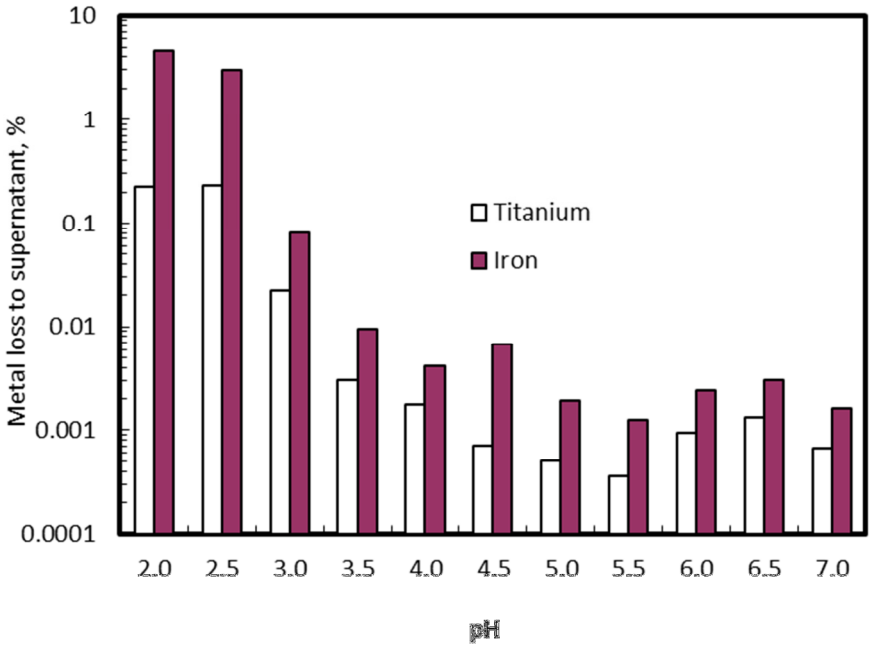

Figure 31: Determination of the optimal hydrolysis pH

4.12 Sulfation Process

The sulfation process was optimised by determining the most effective amount of sulphuric acid used in the process. The stoichiometric amount and an excess of 5–15% was used (excess of H_2SO_4 over the stoichiometric amount required for the reaction to form iron(III) sulfate and titanium(IV) sulfate). The results are presented in Figure 32. The AFDI used was obtained by fusing NaOH:ilmenite mixtures (2:1 mole ratio) at 750 ^{o}C for 1 h.

The results obtained indicate that the sulfation process was not affected by any excess above the stoichiometric amount of sulphuric acid required for the reaction. The relative quantities of iron and titanium did not vary with the addition of any excess of the acid.

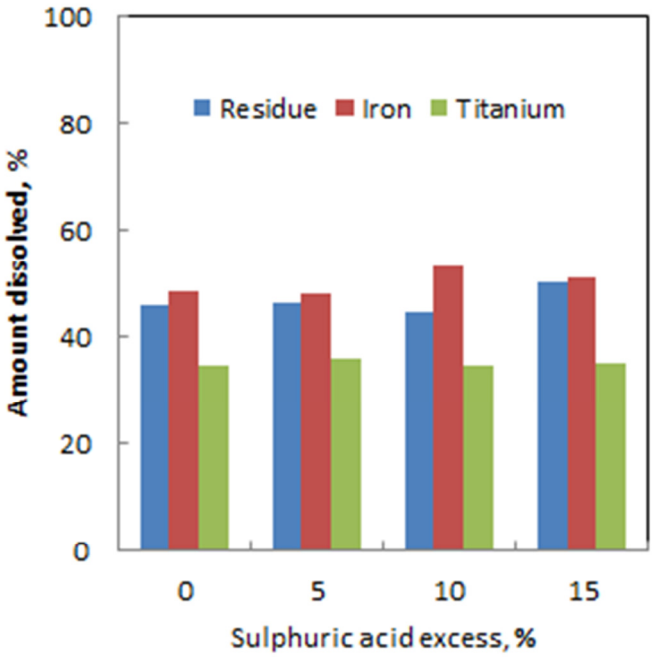

Figure 32: Optimisation of the sulfation process

4.13 Trials with Anatase

There are important world reserves of titanium in the form of anatase, but this mineral is not yet being commercially exploited. Existing commercial routes are incapable of processing such ores (de Matos *et al.*, 2002; Nielsen and Chang, 1996; Paixão and de Mendonça, 1979). In order to assess the applicability of the alkali fusion procedure to such ores, an anatase sample was used to obtain the optimal parameters.

Stoichiometric amounts of anatase reactant were mixed with sodium hydroxide (2:1 NaOH:TiO_2 mole ratio) and subjected to TGA analysis. The aim was to determine the fusion temperature.

The thermogravimetric results (Figure 33) indicated a mass loss from 220 to 850 ^{o}C. The DTG curve indicates two broad peaks, at approximately 670 and 870 ^{o}C. The total mass loss was 20.85%, which corresponds to approximately 97% of the expected total mass loss, calculated from the perspective of the NaOH mass loss. The SDTA curve (from the simultaneous TGA-DTA thermal analyser) shows a peak at 756 ^{o}C.

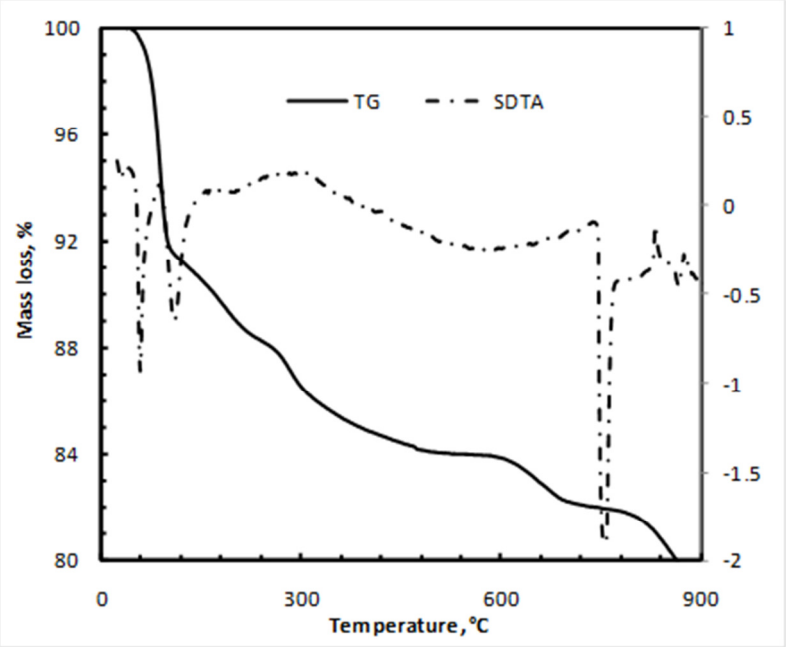

Figure 33: TGA and DTA curves of the alkali fusion reaction

Using the TGA findings, mixtures of NaOH and TiO_2 (anatase, 2:1 mole ratio) were fused at 500, 600, 700 and 800 ^{o}C. The fused samples were subjected to XRD analysis (Figure 34). The XRD patterns revealed the presence of Na_2TiO_3, $Na_{16}Ti_{10}O_{28}$, $Na_8Ti_5O_{14}$ and $Na_2Ti_6O_{13}$ (Figure 34). The polymeric phases are dominant at lower temperatures. The reaction appears to follow the path below:

$$24Na_2O + 30TiO_2 \rightarrow 6Na_8Ti_5O_{14} \rightarrow 3Na_{16}Ti_{10}O_{28} + 6Na_2O \rightarrow$$

$$30Na_2TiO_3 \rightarrow 5Na_2Ti_6O_{13} + 25Na_2O \quad (14)$$

From the economic point of view, phases with the lowest Na:Ti ratio are advantageous. They require less NaOH to combine with Ti in the ore. The most efficient here is $Na_2Ti_6O_{13}$, with a 1:3 atom ratio. It requires 10 moles of NaOH to combine 30 moles of TiO_2, according to equation 14. This phase was obtained above 700 ^oC, according to the XRD results in Figure 34.

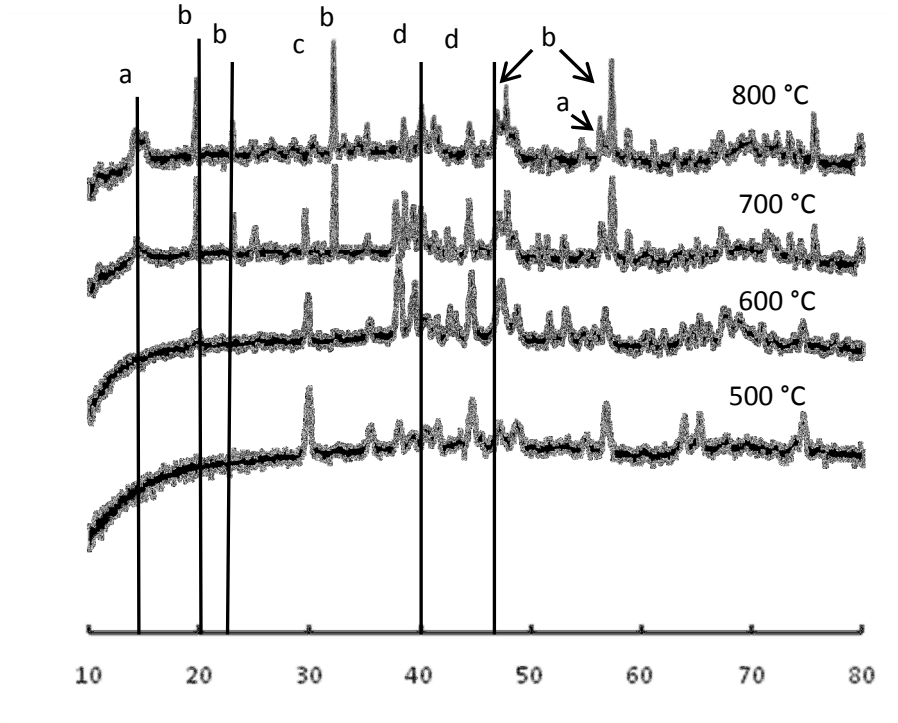

a = $Na_2Ti_6O_3$; b = Na_2TiO_3; c = $Na_8Ti_5O_{14}$; d = $Na_{16}Ti_{10}O_{28}$

Figure 34: XRD patterns of alkali fused anatase (2:1 NaOH:TiO_2 mole ratio)

Optimisation of the processing was conducted by analysing the effect of time and temperature on the process. The effect of time was investigated using a sample fused at 800 ^oC. The results indicated that a maximum recovery can be attained at 120 min. Over 99% of the titania was recovered after this time. Fifty-four percent of the total NaOH used was recovered after this time. The residue reaches its minimum at this point (Figure 34).

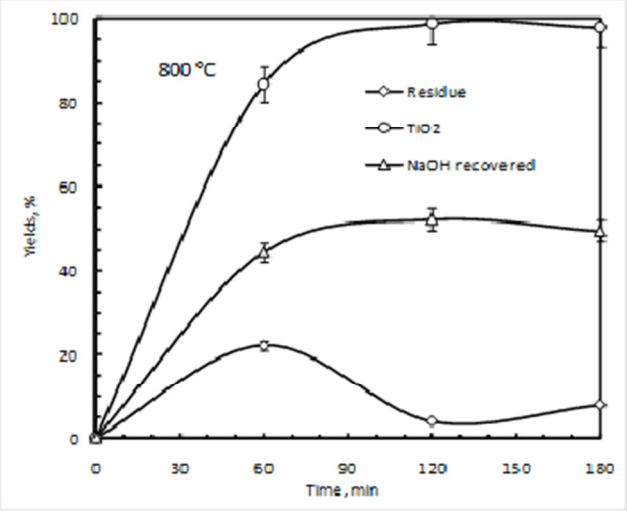

Figure 35: Effect of time on the recovery of titania from anatase ores using the proposed process

The effect of temperature was investigated between 500 and 800 ^{o}C. The results, presented in Figure 36, indicated that at 800 ^{o}C, 84% of the total titania can be recovered from the ore, as well as 45% of the NaOH used.

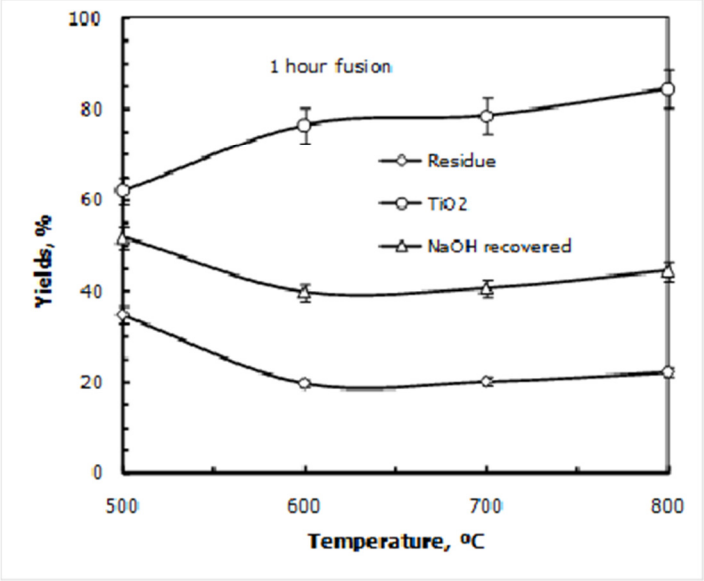

Figure 36: Effect of temperature on the titania recovery from anatase ores using the proposed process

4.14 Summary of the Discussions

In the present work we propose a method of extracting of titanium from titanoferrous minerals. In titanoferrous minerals we include anatase, pseudorutile, altered ilmenite, leucoxene, ulvospinel, pseudobrookite, titanomagnetite and titanohematite, as per Table 1, as well as ilmenite. According to this method titanoferrous mineral is roasted preferable with sodium hydroxide. The fused product is subsequently leached with water, hydrolysed with dilute mineral acid and the residue dissolved in sulphuric acid as indicated in section 2.7.3 of this work.

The proposed process was studied in terms optimum conditions of fusion temperature, mole ratio and time of fusion (duration of the fusion reaction). For the leaching process the slurry density (solid:liquid ratio), temperature of leaching and time were the optimized parameters. For the acid hydrolysis the concentration of the mineral acid was the optimized parameter. The main findings are:

A. Fusion Reaction

- The optimum conditions for the alkali fusion reaction were found to be
  - Temperature – 900 °C
  - Fusion time – 1 h
  - Mole ratio – 2:1 (NaOH:titanoferrous mineral)
  - Particle size – bellow 139 µm

- The overall fusion reaction was found to be

$$28FeTiO_3 + 22Na_2O + 7O_2 \rightarrow 16Na_{0.75}Fe_{0.75}Ti_{0.25}O_2 + 3NaFeTiO_4 + 4Na_2Fe_2Ti_3O_{10} + 4Na_2TiO_3 + 2Na_8Ti_5O_{14} + 10NaFeO_2$$

- The mechanism was predicted to proceed in the following path
    - Initially Na_2TiO_3 and $NaFeO_2$ are produced as result of the high localized concentration of Na^+ in the melt;
    - As the reaction proceeds and the concentration of Na^+ ions in the melt reduces, Na_2TiO_3 polymerises, producing $Na_8Ti_5O_{14}$.
    - Because Na^+ is proportionally insufficient to compensate the demand by Ti^{4+} and Fe^{3+} ions in the event of the ilmenite lattice breaking, Na^+ ions are incorporated into the ilmenite lattice, resulting in the partial substitution of Ti^{4+} and Fe^{3+} ions in the lattice.

Fusion data fitted both contracting area mechanism as well as diffusion. The multiple mechanism of the reaction was proved by the dependence of the activation energy on the heating rate.

B. Leaching

Optimum leaching conditions were found to be

- Temperature – 75 °C
- Slurry density (solid:liquid ratio) – 0.20 g/mL
- Time – 15 min

It was also found that the leaching process obeys the shrinking core mechanism.

C. Hydrolysis

The pH of 7 was found to be the optimum final pH in hydrolysis.

4.15 References

Aminesh, J., Antony, M.P., and Dattatray, T.V., **2007**. US Patent Application No. 20070110647.

Batygin, V.G., **1967**. Formation and some properties of sodium titanates. *Russian Journal of Inorganic Chemistry*, 12(6): 762–767.

Bayer, Von G., Hoffman, W., **1965.** Über Verbindungen vom Na_xTiO_2 – Typ. *Zeitschrift für Kristallographie*, 121: 9–13.

Belyaev, E.K., **1976**. The formation of sodium metatinate in sodium carbonate – Titanium dioxide mixtures. *Russian Journal of Inorganic Chemistry*, 21(6): 830–833.

Belyaev, E.K., Panasenko, N.M., and Linnik, E.V., **1970**. Formation of tetrasodium trititanate in mixtures of sodium carbonate and titanium dioxide. *Russian Journal of Inorganic Chemistry*, **15**(3): 336–338.

Brown, M.E., *et al*., **2000**. Computacional aspects of kinetic analysis. Part I: The ICTAC kinetics project-data, methods and results. *Thermochimica Acta*, 355:125-143.

Chowlu, A.C.K., Reddy, P.K., and Ghoshal, A.K., **2009**. Pyrolytic decomposition and model-free kinetics analysis of mixture of polypropylene (PP) and low density polyethylene (LDPE). *Thermochimica Acta*, 484(1–2): 41–47.

Criado, J.M., **1978**. Kinetic analysis of DTG data from master curves. *Thermochimica Acta*, 24:186-189.

Criado, J.M., Málek, J., and Ortega, A., **1989**. Aplicability of the master plots in kinetic analysis of non-isothermal data. *Thermochimica Acta*, 147:377-385.

De Matos, J. M. J., de Freitas, L. R., and Horta, R. de M., **2002**. Process for the production of titanium concentrate from anatase ores with high utilisation of the iron contents of the ore. US Patent 6 346 223.

Dehghan, R., Noaparast, M., and Kolahdoozan, M., **2009**. Leaching and kinetic modelling of low-grade calcareous spharelite in acidic ferric chloride solution. *Hydrometallurgy*, 96(4): 275–282.

Dellimore, D., Tong, P., and Alexander, K.S., **1996**. The kinetic interpretation of the decomposition of calcium carbonate by use of relationships other than the Arrhenius equation. *Thermochimica Acta*, 282/283: 13–27.

Demirkiran, N., **2008.** Dissolution kinetics of ulexite in ammonium nitrate solutions. *Hydrometallurgy*, 95(3–4): 198–202.

Dickinson, F.C., and Heal, G.R., **1999**. Solid-liquid diffusion controlled rate equations. *Thermochimica Acta*, 340–341: 89–103.

Farmer, V.C., **1974**. The infrared spectra minerals, V.C. Farmer Edition. Mineralogical Society Monograph, 4. Mineralogical Society, London.

Foley, E., and MacKinnon, K.P., **1970.** Alkaline roasting of ilmenite. *Journal of Solid State Chemistry*, 1: 566–575.

Gabelica-Robert, M., and Tarte, P., **1981**. Vibrational spectrum of fresnoite ($Ba_2TiOSi_2O_7$) and isostructural compounds. *Physics and Chemistry of Minerals*, 7: 26–30.

Habashi, F. (Ed.), **1997.** Titanium. In: *Handbook of Extractive Metallurgy, Vol. II*. Weinheim, Germany: Wiley-VCH, pp 1129–1180

Harrison, L.G., **1969**. The Theory of Solid Phase Kinetics. In: Bamford, C.H., and Tipper, C.F.H., *Comprehensive Chemical Kinetics*, 2nd edition, vol. 2, Elsevier Publishing Company, pp. 377-458.

Hollitt, M.J., McClelland, R.A., and Tuffley, J.R., **2002**. Upgrading titaniferous materials. US Patent Application No. 20020104406.

Jambor, J.L., Dutrizac, J.E., **1998**. Occurrence and constitution of natural and synthetic ferrihydrite, a widespread iron oxyhydroxide. *Chemical Reviews*, 98 (7): 2549–2585.

Jin, D., Yu, X., Yue, L., and Wang, L., **2009**. Decomposition kinetics study of AlOOH-coated calcium carbonate. *Materials Chemistry and Physics*, 115(1): 418–422.

Johansson, M., **2007**. Screening of oxygen-carrier particles based on iron-, manganese-, copper- and nickel oxides for use in chemical-looping technologies. PhD. Thesis Chalmers University of Technology, Goteborg –Sweeden.

Khawam, A., and Flanagan, D.R., **2005**. Role of isoconversional methods on varying activation energies of solid state kinetics. II. Non-isothermal kinetic studies. *Thermochimica Acta*, 436: 101–112.

Kuhn, A., García-Alvarado, F., Morán, E., Alario-Franco, M.A., and Amador, U., **1996**. Structural effects of sodium extraction on $Na_xFe_xTi_{2-x}O_4$ single crystals. *Solid State Ionics*, 86–88: 811–818.

Lahiri, A., Kumari, E. J., and Jha, A., **2006**. Kinetic studies on the soda-ash roasting of titanoferous ores for the extraction of TiO_2. *Proceedings of theSohn International Symposium. Advanced Processing of Metals and Materials. Vol. 1: Thermo and Physicochemical Principles: Non-Ferrous High-Temperature Processing*, pp 115–123.

Lasheen, T.A., **2008**. Soda ash roasting of titania slag product from Rosetta ilmenite. *Hydrometallurgy*, 93:124-128.

Leion, H., Lyngfelt, A., Johansson, M., Jerndal, E., and Mattisson, T., **2008**. The use of ilmenite as an oxygen carier in chemical-looping combustion. *Chemical Engineering Research and Design*, 86:1017-1026.

Li, C., Reid, A.F., and Saunders, S., **1971**. Nonstoichiometric alkali ferrites and aluminates in the systems $NaFeO_2 – TiO_2$, $KFeO_2 – TiO_2$, $KAlO_2 – TiO_2$, $KAlO_2 – SiO_2$.*Journal of Solid State Chemistry*, 3: 614–620.

Licht, S., Yang, L., and Wang, B., **2005**. Synthesis and analysis of Ag_2FeO_4Fe(VI) ferrate super-iron cathodes. *Electrochemistry Communications*, 7: 931–936.

Lick, I.D., Villalba, M.L., and Gavernet, L., **2012**. Synthesis of diketopiperazine: A kinetic study by means of thermoanalytical methods. *Thermochimica Acta*, 527:143-174.

Maitra, S., Chakrabarty, N., and Pramanik, J., **2008**. Decomposition kinetics of alkaline earth carbonates by integral approximation method. *Cerâmica*, 54: 268–272.

Manikandan, G., Jayabharathi, J., Rajarajan, G., and Thanikachalam, V., **2011**. Kinetics and vaporization of anil in nitrogen atmosphere – non-isothermal condition. *Journal of King Saud University – Science*, doi: 10.1016/j.jksus.2011.04.002 (in press).

Méndez-Vivar, J., Mendoza-Serna, R., and Valdez-Castro, L., **2001**. Control of the polymerization process of multicomponent (Si, Ti, Zr) sols using chelating agents. *Journal of Non-Crystalline Solids*, 288:200-209.

Muroya, M-A., **1999**. Correlation between the formation of silica skeleton structure and Fourier transform reflection infrared absorption spectroscopy spectra. *Colloids and Surfaces A: Physicochemical and Engineering Aspects*, 157: 147–155.

Nagarajan, S., and Rajendra, N., **2009**. Surface characterization and electrochemical behaviour of porous titanium dioxide coated 316L stainless steel for orthopaedic applications. *Applied Surface Science*, 255:3927-3932.

Nielsen, R., and Chang, T.W. **1996**. In: Elvers, B., Hawkins, S. and Schultz, G. (Eds), *Ullman's Encyclopaedia of Industrial Chemistry,* 5th edition, Vol. A28, Weinheim, Germany, Wiley VCH, pp 543–567 and 95–122.

Noisong, P., Danvirutai, C., Srithanratana, T., and Boonchom, B., **2008**. Synthesis, characterization and non-isothermal decomposition kinetics of manganese hypophosphite monohydrate. *Solid State Sciences*, 10: 1598–1604.

Paixão, J. M. J., and de Mendonça, P. A. F., **1979**. Process for concentration of titanium containing anatase ore. US Patent 4 176 159.

Peng, G.-W., and Liu, H.-S., **1995**. FT-IR and XRD characterization of phase transformation of heat-treated synthetic natisite ($Na_2TiOSiO_4$) powder. *Materials Chemistry and Physics*, 42: 264–275.

Ratnasamy, P., Srinivas, D., and Knözinger, H., **2004**. Active sites and reactive intermediates in titanium silicate molecular sieves. *Advances in Catalysis*, 48:1-169.

Reid, A.F., and Sienko, M.J., **1967**. Some characteristics of sodium titanium bronze and related compounds. *Inorganic Chemistry*, 6(2): 321–324.

Ryskin, Ya.I, **1974**. The Infrared Spectra of Minerals. Mineralogical Society Monograph 4. Farmer, V.C., edition. Adlard and Son Ltd., London.

Roth, R.S., Negas, T., and Cook, L.P. (Eds), **1981**. *Phase Diagrams for Ceramists*, Columbus, US: American Ceramic Society, Figs. 5123, 5124 and 5338.

Sbirrazzuoli, N., Vicent, L., and Vyazovkin, S., **2000**. Comparison of several computational procedures for evaluating the kinetics of thermally stimulated condensed phase reactions. *Chemometrics and Intelligent Laboratory Systems*, 54:53-60.

Sertkol, M., Köseoğlu, Y., Baykal, A., Kavas, H., and Basaran, A.C., **2009**. Synthesis and magnetic characterisation of $Zn_{0,6}Ni_{0,4}Fe_2O_4$ nanoparticles Via a polyethylene glycol-assisted hydrothermal route. *Journal of Magnetism and Magnetic Materials*, 321: 157–162.

Tarte, P., Cahay, R., and Garcia, A., **1979**. Infrared Spectrum and structural role of titanium in synthetic Ti-garnets. *Physics and Chemistry of Minerals*, 4: 55–63.

Vicente-Rodríguez, M.A., Suarez, M., Banãres-Munõz, M.A., Lopez-Gonzalez, J. de D.,**1996**. Comparative FT-IR study of removal of octahedral of cations and structural modifications during acid treatment of several silicates. *Spectrochimica Acta A*, 52: 1685–1694.

Vyazovkin, S., Burnham, A.K., Criado, J.M., Pérez-Maqueda, L.A., Popescu, C., and Sbirrazzuoli, N., **2011**. ICTAC kinetics committee recomendations for performing kinetic computations on termal analysis data. *Thermochimica Acta*, 520:1-19.

Wilburn, F.W., **2000**. Kinetics of overlapping reactions.*Thermochimica Acta*, 354: 99–105.

Xu, Z., Wang, J., Shao, H., Tang, Z., and Zhang, J., **2007**. Preliminary investigation on the physicochemical properties of calcium ferrate (VI). *Electrochemistry Communications*, 9: 371–377.

Zhang, J-Q., Hong-xu, G., Li-Hong, S., Rong-Zu, H., Feng-qi, Z., and Bo-Zhou, W., **2009**. Non-isothermal thermal decomposition reaction kinetics of 2-nitroimino-5-nitro-hexahydro-1,3,5-triazine. *Journal of Hazardous Materials*, 163(1–3): 205–208.

Zhang, M., Salje, E.K.H., Ewing, R.C., Farnan, I., Ríos, S., Schlüter, J., and Leggo, P., **2000**. Alpha-decay damage and recrystallization in zircon: Evidence for an intermediate state from infrared spectroscopy. *Journal of Physics: Condensed Matter*, 12: 5189–5199.

5 Conclusions

Titania is an important white pigment and opacifier for various applications. It is obtained from rutile, ilmenite and from synthetic sources, such as synthetic rutile and titanium slag. However, there are several other titanium minerals, as well as some ilmenite ores, which cannot be exploited due to the lack of appropriate technology. Such minerals include anatase, perovskite, sphene, titanomagnetites and low-grade ilmenites with a higher content of quality-degrading impurities.

Existing technologies face numerous challenges related to their (i) inability to treat most of the existing ores, (ii) higher energy consumption, (iii) high waste generation, and (iv) generation of greenhouse gases. Another important factor in the titania industry is the decrease in availability of reachable reserves and reserves free of radioactive impurities. Therefore, new processes for titania processing have to be found.

The aim of this work was to develop a new route for upgrading titania raw materials into pigment. The route proposed here entails: the use of sodium hydroxide to reduce iron content, and to immobilise or extract radioactive impurities; wet treatment to hydrolyse titanium oxide and iron oxide; and sulfation to extract titanium. This process is able to treat a broad range of ores.

There are three critical stages in the process:

1. **Fusion** – sodium hydroxide reacts with ilmenite.
2. **Leaching** – water is used to leach out impurities and recover sodium hydroxide.
3. **Sulfation** – titanium and iron are solubilised.

Further, the sulfate solution is hydrolysed to copperas and titania, via the normal sulfate process. Alternatively, hydrolysed AFDI can be introduced into the chloride process as titanium

feedstock after calcination. Each of these steps was separately studied and the following conclusions were drawn.

5.1 Fusion Step

Economic conditions necessitate the use of smaller amounts of the alkali while releasing the highest quantity of titanium. This is consistent with the formation of ternary phases ($Na_2O.Fe_2O_3.TiO_2$). The mole ratio of 2:1 (NaOH:ilmenite) was found to be the most effective in producing ternary phases. Using this mole ratio, 0.41 mass units were released per unit mass of sodium hydroxide, fusing at 900^{o}C, for 1 h. The theoretical limit is 0.53 units for this mole ratio.

When the aforementioned conditions (2:1 mole ratio, 900 ^{o}C, 1 h) were used for fusion, $Na_{0.75}Fe_{0.75}Ti_{0.25}O_2$, $NaFeTiO_4$ and $Na_2Fe_2Ti_3O_{10}$ were the ternary phases identified in the fused products. Binary phases were also present; they accommodate the surplus titanium or iron whenever the atom ratio of Fe:Ti is different from 1:1. Na_2TiO_3, $Na_8Ti_5O_{14}$ and $NaFeO_2$ were identified in the product spectrum.

Fusion mole ratios higher than 2:1 (NaOH:ilmenite) produced essentially binary phases. Na_2TiO_3 and $NaFeO_2$ are binary phases the observed. $NaTiO_2$ was observed in the products when fusions were conducted for 1 h or less of fusion time. The formation of $NaTiO_2$ results from the non-availability of oxygen to act as oxidant in the iron oxidation reaction. With short periods of fusion (less than 1 h) binary phases were also dominant. This was also observed when fusions were conducted below 600 ^{o}C.

When mole ratios below 2:1 (NaOH:ilmenite) were used at 850 ^{o}C for 1 h in fusion, $Na_2Fe_2Ti_3O_{10}$ and $NaFeTiO_4$ were the sole ternary phases in the product spectrum. Fusions conducted below 850 ^{o}C under these conditions produced binary phases as well as unreacted ilmenite. Although the reaction was completed after 1 h at 850 ^{o}C in these non-stoichiometric conditions, only ≈ 30% of the total titanium was recovered using a 1:1 mole ratio.

The maximum yield (81% of total titanium) was achieved at 900 ^{o}C, using a 2:1 (NaOH:ilmenite) mole ratio, for 1 h of fusion time. Increasing the fusion time did not result in significant changes in the titanium yield. The fusion reaction appeared to be independent of the ilmenite particle size above 750 ^{o}C.

When anatase reactant was used to resemble an anatase ore, four phases were obtained, namely $Na_2Ti_6O_3$, Na_2TiO_3, $Na_8Ti_5O_{14}$ and $Na_{16}Ti_{10}O_{28}$. The highest recoveries of titanium were obtained after fusing at 800 ^{o}C for 2 h, and with a 1:1 (NaOH:TiO_2) mole ratio. Approximately 100% of titanium was recovered under these conditions.

5.2 Leaching Step

It was found that the leaching step was dependent on time, solid:liquid ratio and temperature. The optimum conditions for solid:liquid ratio, time and temperature were found to be 0.20, and 15 min at 75 ^{o}C respectively.

5.3 Other Steps

Other optimised steps were acidic hydrolysis and sulfation. Acidic hydrolysis was controlled by the relative amount of iron and titanium in solution. It was found that less than 1% was dissolved between 3 and 7 in pH units. Higher pH values are recommended since less acid will be used.

Any excess of sulphuric acid in the sulfation step proved to be unnecessary. No significant changes were observed in the amount of dissolved iron and titanium. Therefore the stoichiometric amount can be used in the sulfation process.

5.4 Recommendations

Our work was aimed to develop a route which will broaden the spectrum of titanium minerals that could be used in the sulfate process. The main problems of the process are (i) the high amount of non-saleable by-product iron sulfate; (ii) the inability of the process to deal with radioactive impurities.

Although we might claim success in broadening the spectrum of titanium minerals that can be used in titania production via sulfate route, we are aware that we were unable to tackle the issue of high amounts of iron sulfate. Our process also produces amounts of this by-product. There is therefore a challenge of transforming the iron sulfate by-product in a more useful product. This can be attained by encountering new uses or else to transform it in new chemicals that can find a wider market.

The second problem, of the radioactive impurities, although we might have been successful on targeting we were unable to certify the existence of phases containing these impurities. The idea was to produce phases that would make possible the separation of radionuclides from the product and from the waste stream.